Suspension of bed material over sand bars in the Lower Mississippi River and its implications for Mississippi delta environmental restoration

Michael T. Ramirez[1] and Mead A. Allison[1,2,3]

Received 6 July 2012; revised 12 April 2013; accepted 21 April 2013; published 18 June 2013.

[1] Understanding specific pathways for sand transport in the lower reaches of large rivers, including the Mississippi, is a key for addressing multiple significant geologic problems, such as delta building and discharge to the oceans, and for environmental restoration efforts in deltaic environments threatened by rising sea levels. Field studies were performed in the Mississippi River 75–100 km upstream of the Gulf of Mexico outlet in 2010–2011 to examine sand transport phenomena in the tidally affected river channel over a range of discharges. Methods included mapping bottom morphology (multibeam sonar), cross-sectional and longitudinal measurements of water column velocity and acoustic backscatter, suspended sediment sampling, and channel-bed sampling. Substantial interaction was observed between the flow conditions in the river (boundary shear stress), channel-bed morphology (size and extent of sandy bedforms), and bed material sand transport (quantity, transport mode, and spatial distribution). A lateral shift was observed in the region of maximum bed material transport from deep to shallow areas of subaqueous sand bars with increasing water discharge. Bed material was transported both in traction and in suspension at these water discharges, and we posit that the downriver flux of sand grains is composed of both locally- and drainage basin-sourced material, with distinct transport pathways and relations to flow conditions. We provide suggestions for the optimal design and operation of planned river diversion projects.

Citation: Ramirez, M. T., and M. A. Allison (2013), Suspension of bed material over sand bars in the Lower Mississippi River and its implications for Mississippi delta environmental restoration, *J. Geophys. Res. Earth Surf.*, *118*, 1085–1104, doi:10.1002/jgrf.20075.

1. Introduction

[2] With widespread acknowledgement of recent climate change [*Crutzen*, 2002], accelerating sea-level rise [*Church and White*, 2006], and projections of future changes to the climate system [*IPCC*, 2007] comes the understanding that low-lying coastal areas are at risk in the coming century and beyond. Mitigating the threat to human populations of the deltaic plains of many large rivers (e.g., Amazon, Ganges-Brahmaputra, Mississippi, Mekong, Nile, Yangtze, and Yellow) is complicated by the low elevation and population density of these areas and the history of human alteration to the natural sedimentary systems upstream of and within deltaic estuaries [*Bianchi and Allison*, 2009]. The history of human alteration to riverine sedimentary systems is well documented [*Syvitski*, 2005] and includes modulation of sediment loads through land use (e.g., drainage-basin deforestation increases runoff), reservoir construction (e.g., trapping sediment from being transported downstream), flood control measures (e.g., artificial levees and diversions), and navigational modifications (e.g., dredging, "fixing" channel planforms).

[3] Environmental restoration efforts in fluvial-deltaic systems must take into account how human alteration affects fundamental physical processes such as hydrodynamics, sediment transport, and sediment supply and how these systems differ from those with natural conditions. One example is the recent work to reestablish natural habitats in the Colorado River downstream of the Glen Canyon Dam [*Melis*, 2011]. The Colorado River is highly regulated and the Glen Canyon Dam has drastically reduced historic sediment supply to the reach downstream for over half a century, leading to scouring of sand bars in the channel [*Topping et al.*, 2000]. Recent experiments aiming to develop methods for restoring sand bar habitats have determined that controlled water releases from the dam can be timed to coincide with sand supply maxima from tributaries downstream of the dam to distribute this sand to channel bars [*Melis*, 2011]. This study is an example of how understanding the transport pathways of bed-material load and wash load can inform river management programs, taking into account the complicated effects of human alteration on the linkage between sediment supply and transport.

[1]Institute for Geophysics, Jackson School of Geosciences, The University of Texas at Austin, Austin, Texas, USA.
[2]Now at The Water Institute of the Gulf, Baton Rouge, Louisiana, USA.
[3]Now at Department of Earth and Environmental Sciences, Tulane University, New Orleans, Louisiana, USA.

Corresponding author: M. T. Ramirez, Institute for Geophysics, Jackson School of Geosciences, The University of Texas at Austin, 10100 Burnet Road Austin, TX 78758, USA. (m.ramirez@utexas.edu)

2169-9003/13/10.1002/jgrf.20075

[4] The interaction between sediment supply and transport in a highly altered system such as the lower Mississippi River complicates efforts to restore the degraded deltaic wetlands of Louisiana. Coastal land loss is a major problem facing the low-elevation deltaic coast of southeastern Louisiana: wetlands are presently being lost at an average rate of 26–30 $km^2 yr^{-1}$ [*Barras et al*., 2003] due to artificial limiting of overbank river flow and a historical decline in sediment supply from impoundment upstream [*Meade and Moody*, 2010], coupled with eustatic sea-level rise, extreme regional subsidence rates [*Penland and Ramsey*, 1990; *Day et al*., 2000; *Morton et al*., 2006; *Törnqvist et al*., 2008], and frontal and cyclonic storm wave erosion [*Day et al*., 2007]. Under natural conditions, the loss of elevation due to this relative sea-level rise would be offset by riverine sediment delivered to the wetlands by periodic overbank flooding and crevasse splay deposition.

[5] One method proposed for replenishment of Louisiana deltaic marshes is the construction of uncontrolled or controlled river diversion structures [*Gagliano et al*., 1981; *Kim et al*., 2009; *Allison and Meselhe*, 2010; *LACPRA*, 2012], through which turbid river water can bypass the levee system and deposit its sediment load in surrounding interdistributary areas. Capturing the suspended sand load is thought to be particularly crucial in designing and operating land-building river diversions, as the sand provides a stable, wave-resistant substrate upon which fine muds and biomass can accumulate [*Day et al*., 2000]. Management of such large-scale river diversions will require careful monitoring of sand and fine sediment transport through the nearby river reaches and an in-depth understanding of how the sand is sourced both locally (from the channel bed of a nearby bar or one immediately upriver) and from the drainage basin (wash load) in order to maximize sand capture rates. It is also important to note that the finer (silt and clay) sediment is the majority of the river's total sediment load [*Meade and Moody*, 2010; *Allison et al*., 2012], and this material is sourced primarily from the drainage basin [*Biedenharn et al*., 2000]. A number of diversion projects are planned in the tidal reach of the Mississippi River [*LACPRA*, 2012], yet little is known about how land-building diversions will interact with the sedimentary system of the river. It also remains unclear how these diversions will affect ongoing sand mining projects that deliver dredged sediment to interdistributary wetlands: whether the diversions will capture sand that would be replenishing dredge borrow areas, or whether the two coastal restoration methods can coexist by targeting complementary sediment sources. As deltaic and other coastal wetlands around the world are threatened in the 21st century [*Nicholls*, 2004; *Church and White*, 2006; *Syvitski et al*., 2009], the quantification of source, replenishment rates, and availability in suspension of Mississippi River sediment resources to help design measures to combat land loss may serve as a model to international communities facing similar problems.

[6] The primary objective of the present study is to examine the dynamic links between sediment supply and transport in the tidal reach of the Mississippi River utilizing a coordinated set of field measurements at distinct water discharges. Data from nearby river monitoring stations operated by the United States Geological Survey (USGS) and United States Army Corps of Engineers (USACE) are integrated with physical sampling of river water and sediment, and geophysical techniques to: (1) demonstrate the effect of river flow on the morphology of subaqueous channel bars; (2) quantify the relative contributions of upstream and local (bed material) sand and fine sediment to suspended sediment loads and the processes responsible for suspending this material; and (3) assess the implications of ongoing and planned coastal restoration practices on the Mississippi River sedimentary system.

2. Background

2.1. Near-Bed Sediment Transport in the Tidal Reaches of Large Rivers

[7] Particulate transport in lowland, sand bed rivers can be divided into two components: wash load and bed material load. *Wash load* comprises sedimentary grains finer than those present in the channel bed [*Einstein*, 1950] and is transported completely in suspension [*Gomez*, 1991; *Church*, 2006]. *Bed material load* is the movement of grain sizes found in the bed of a river reach [*Einstein*, 1950] and its transport has been related to physical characteristics of flow in the local reach, such as total water discharge, current velocity, and shear stress [*Gomez*, 1991; *Church*, 2006]. In the case of the tidal reach of the Mississippi River, the wash load mainly consists of silts and clays [*Biedenharn et al*., 2000], a portion of which are deposited seasonally at low discharge in the tidal-estuarine reach of the channel, and therefore may temporarily be considered bed material. These particles are remobilized and not deposited at higher flows [*Galler and Allison*, 2008]. Sand-sized (>62.5 μm) particles making up the Mississippi River channel bed may be transported as bedload—rolling, sliding, and saltating [*Gomez et al*., 1989]—or as suspended load when upward forces imparted to particles by the flow exceed the gravitational force on the particles [*van Rijn*, 1984; *Garcia and Parker*, 1991]. The transport mode of sand is a function of flow conditions.

[8] Large sand bedforms with wavelengths (up to 100 s of m) significantly longer than flow depths (10 s of m) have been observed in large lowland rivers around the world (e.g., Fraser River, *Kostaschuk and Villard* [1996]; Brahmaputra River, *Roden* [1998]; Rhine River, *Carling et al*. [2000]; Nile River, *Abdel-Fattah et al*. [2004]; Mississippi River, *Nittrouer et al*. [2008]; Río Paraná, *Shugar et al*. [2010]). Dunes in the tidal reach of the Mississippi River are persistent over a range of water discharges and vary from 0.5–2.5 m high and 10–20 m long at low discharge (11,000 $m^3 s^{-1}$) to 5–10 m high and 75–150 m long at high discharge (34,000 $m^3 s^{-1}$; *Nittrouer* [2006]; *Allison et al*. [2013]). These dunes are asymmetrical and display higher lee slopes than stoss slopes, though all slopes are much less than the angle of repose. Additionally, large areas of the channel in meander segments are devoid of any alluvial sand cover [*Nittrouer*, 2006; *Nittrouer et al*., 2008, 2011b].

[9] It has been shown that flows over subaqueous dune fields (a nearly ubiquitous feature of sandy lowland rivers) are characterized by turbulent structures in the bottom boundary layer [*Roden*, 1998; *Kostaschuk*, 2000; *Shugar et al*., 2010], which may or may not involve flow separation in the leeside of bedforms, depending on the geometry of the

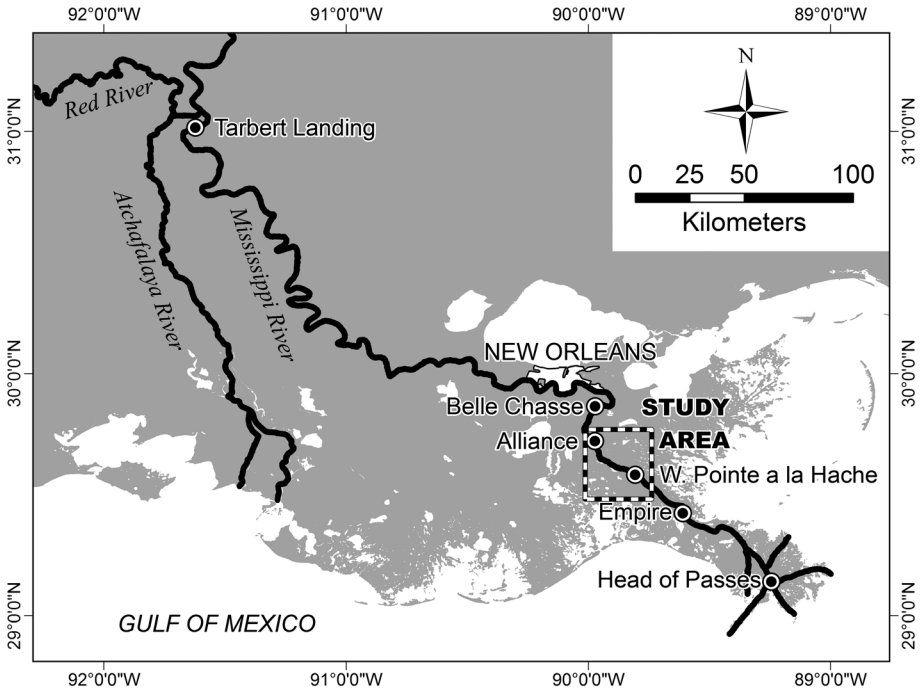

Figure 1. Map of southeastern Louisiana, with locations of Mississippi River study area and monitoring stations referenced in the text.

dunes [*Best and Kostaschuk*, 2002]. Eddies generated in this boundary layer are associated with turbulent energy production and dissipation [*Engelund and Fredsøe*, 1982]. These structures can exhibit instantaneous streamwise and vertical velocities that diverge substantially from time-averaged vector values and produce fluctuations in stress within the bottom boundary layer [*Lapointe*, 1992; *Bennett and Best*, 1995]. Several studies have recognized this turbulence in the velocity fields of natural and laboratory flows and have linked the turbulence intensities generated by these motions with the suspension and transport of bed material [*Bennett and Best*, 1995; *Roden*, 1998; *Kostaschuk*, 2000; *Venditti and Bennett*, 2000; *Best*, 2005; *Shugar et al*., 2010].

2.2. Study Area

[10] The Mississippi River flows nearly 3000 km from northern Minnesota to southern Louisiana, and when combined with its tributaries, drains an area over 3×10^6 km^2 [*Mossa*, 1996]. The USACE monitoring station at Tarbert Landing, MS, *RK* 493 (Figure 1; river kilometers, *RK*, denote distance upstream of the Mississippi River mouth at Head of Passes) has recorded a mean daily water discharge of 14,307 m^3 s^{-1} during the period 1961–2010, with representative high and low discharges (calculated as the mean of highest discharge from each year and the mean of lowest discharge from each year) of 30,261 m^3 s^{-1} and 5334 m^3 s^{-1}, respectively (data available at www.mvn.usace.army.mil/cgi-bin/wcmanual.pl?01100). In the 1961–2010 time period, the Mississippi River at Tarbert Landing exhibited high discharge (greater than mean) an average of 153 days per year (generally December to June), typically with several individual flood peaks lasting 2–4 weeks each.

[11] The sediment discharge of the Mississippi River has been shown to vary widely with water discharge and distance downstream [*Mossa*, 1996; *Meade and Moody*, 2010; *Allison et al*., 2012]. Suspended sediment discharges recorded at Tarbert Landing for the above-mentioned low, mean, and high water discharges were 86,000 tons per day (T d^{-1}), 380,000 T d^{-1}, and 500,000 T d^{-1}, respectively. There is an offset, however, in the relative timing of water discharge and suspended sediment maxima [*Mossa*, 1996; *Allison et al*., 2012], which has been attributed to (1) the hysteresis cycle that results in a pulse of wash load during initial upland floodplain inundation, and in the lowland reach to (2) the resuspension of fine sediment stored on the channel floor and in vegetated areas inside the artificial levees (battures) that is remobilized as water levels and velocities increase, and is depleted before the period of maximum discharge [*Galler and Allison*, 2008; *Allison and Meselhe*, 2010].

[12] The area of the present study is in the tidal reach of the river downstream of New Orleans, LA between river kilometers 74 and 105 (Figures 1 and 2). This reach of the river is relatively straight compared to the sinuous planform upstream of New Orleans (Figure 1). Channel morphology in the reach downriver of New Orleans exhibits a pattern of alternating, 1–5 km long bank-attached sand bars in the straightest segments and deep, erosional pools in bend segments [*Nittrouer et al*., 2011b]. Average channel width in the study area is 825 m and typical channel depths range from over 40 m in the thalweg, to ca. 18 m over the top of alternate bars, and less than 1 m in vegetated areas along the banks (battures). Water surface slopes for this reach (calculated using water stage data from USACE gages at Alliance—*RK* 100, West Pointe a la Hache—*RK* 77, and Empire—*RK* 47; Figure 1) range over an order of magnitude: from 1.7×10^{-6} at low discharge, to 3.2×10^{-6} at mean discharge, and 1.9×10^{-5} at high discharge. Depth-averaged stream velocities measured at the USGS Belle Chasse station (*RK* 121, Figure 1) for low, mean, and high discharges are 0.37, 0.85, and 1.65 m s^{-1}, respectively.

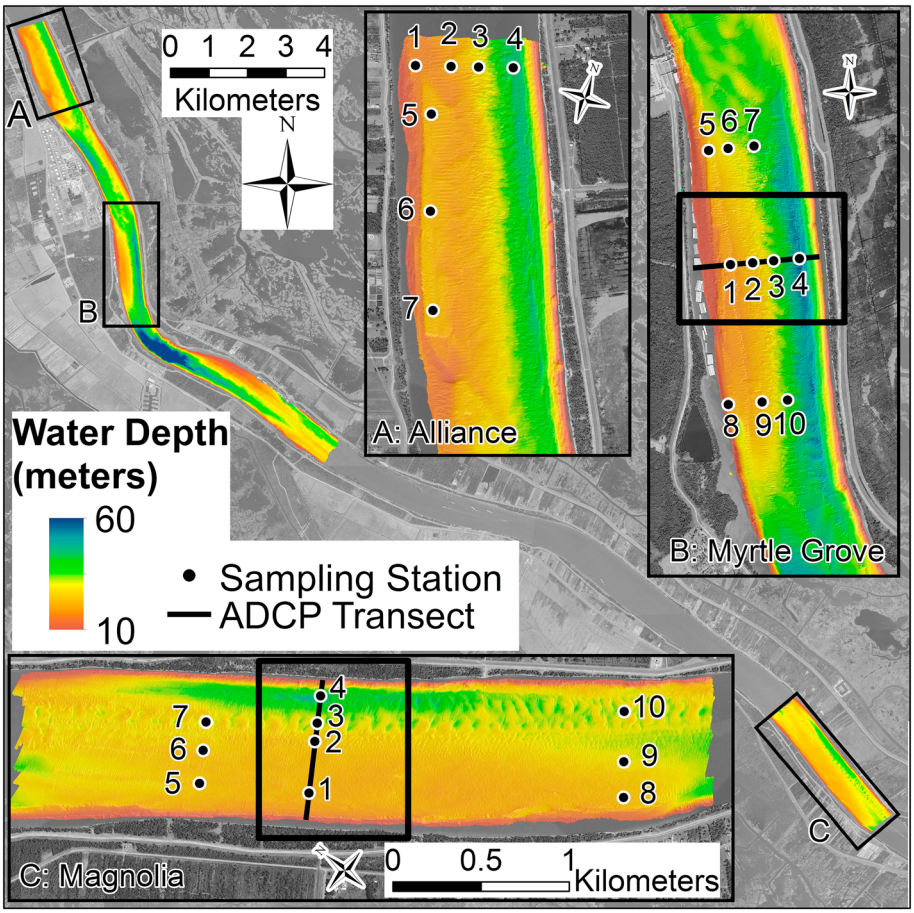

Figure 2. Map of the Mississippi River channel study sites, with inset multibeam bathymetric maps created during the present study. Sampling stations at each of the three study sites (points), the locations of ADCP cross sections (lines), and the limits of bedform transport study grids (boxes) are given in the inset maps. Note north arrows. All inset maps at same scale.

[13] Tidal modulation of stream velocities and discharges (as calculated from 15 min-interval data at Belle Chasse and hourly data from Alliance, West Pointe a la Hache, and Empire) ranges ±10% of the mean at high discharge and ±44% at low discharge. Tidal modulation of water surface height ranges ±2% of the mean at high discharge and ±12% at low discharge. Tidal modulation of water surface slope ranges ±3% of the mean at high discharge and ±15% at low discharge. The greatest stream velocities and water discharges coincide with the falling tide. *Galler and Allison* [2008] describe tidal effects and estuarine processes in the lowermost reach of the Mississippi River, where saline bottom-water intrusion was observed 19 km upstream of Head of Passes at a water discharge of 7930 $m^3 s^{-1}$ but not at a discharge of 10,500 $m^3 s^{-1}$. An earthen structure has been emplaced in the river thalweg by the USACE at *RK* 116 (i.e., upstream of the present study area) on two occasions in the last 25 years to prevent the intrusion of saltwater and the contamination of New Orleans drinking water during extreme low discharges (<4200 $m^3 s^{-1}$; *Allison and Meselhe* [2010]).

[14] Bedform transport rates measured in prior studies of the tidal reach of the Mississippi River display a close correlation with water discharge. *Nittrouer et al*. [2008] measured an exponential increase in rates of bedform transport over a range of water discharges at several locations between New Orleans (*RK* 167) and Venice (*RK* 8), with specific values varying from less than 1000 T d^{-1} to greater than 50,000 T d^{-1} at water discharges of 6000 $m^3 s^{-1}$ and 34,000 $m^3 s^{-1}$, respectively. *Nittrouer et al*. [2011a] calculated no sand in suspension at a water discharge of 11,300 $m^3 s^{-1}$ and a suspended sand discharge of 126,000 T d^{-1} during a high water discharge of 38,400 $m^3 s^{-1}$. These measurements imply that bedload contributions to total (sand, silt, and clay) sediment discharge range from 1% to 10% between low and high water discharge. Conversely, bedload transport may make up 100% of total sand transport during low water discharge when there is not enough flow energy to suspend sand. At high discharge, when substantial amounts of sand are in suspension, bedload transport contributes about 30% to total sand discharge [*Nittrouer et al*., 2011a]. Given the 10% tidal variation in high water discharge observed at Belle Chasse and the exponential relation between bedform transport of *Nittrouer et al*. [2008], a nearly ±50% tidal variation in bedform transport may be expected at high discharge. This same tidal variability in high water discharge may produce a

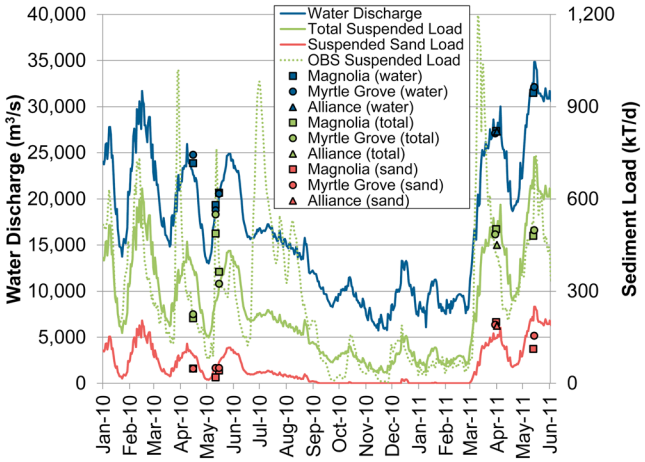

Figure 3. Daily water discharge (blue line), ratings-curve derived sediment loads (total suspended sediment-green line; suspended sand-red line) from *Allison et al*. [2012], and calibrated optical backscatterance sensor (OBS) suspended sediment record (dashed green line) for the USGS monitoring station at Belle Chasse, LA from January 2010 to June 2011 (location in Figure 1). Point values are measurements of water discharge (blue), total suspended sediment (green), and suspended sand (red) made at Magnolia (squares), Myrtle Grove (circles), and Alliance (triangles) during the study periods in April 2010, May 2010, March 2011, and May 2011.

suspended sand discharge tidal variability of ±34% about the mean according to the rating curves produced by *Allison et al*. [2012].

3. Methods

3.1. Field Surveys

[15] Field studies were conducted at the Myrtle Grove and Magnolia study sites (locations in Figure 2) on 12–16 April 2010; 11–15 May 2010; 29 March–1 April 2011; and 12–14 May 2011. The April 2010 study period occurred during a falling hydrograph, with discharge decreasing from 23,760 $m^3 s^{-1}$ to 22,486 $m^3 s^{-1}$. The May 2010 study period was carried out during a rising hydrograph: discharge increased from 18,578 $m^3 s^{-1}$ to 20,419 $m^3 s^{-1}$ during the 5 day study. The March 2011 study period occurred at the peak of a flood wave, with discharge ranging from 27,159 $m^3 s^{-1}$ to 27,499 $m^3 s^{-1}$. The May 2011 study period coincided with peak flood conditions of about 32,000 $m^3 s^{-1}$. Discharges are reported from the USGS Belle Chasse station (Figure 3) even though measurements were made at the study sites because the USGS data are collected continuously at 6 min intervals by horizontal acoustic Doppler current profiler (ADCP) and are daily averaged to remove tidal modulation. All surveys were conducted aboard the 7 m R/V *Lake Itasca* owned by the University of Texas Institute for Geophysics.

[16] Study sites were examined using (1) cross-sectional and stationary ADCP measurements, (2) multibeam sonar basemapping and bedform transport measurements, and (3) sampling of river water and bed material by isokinetic point sampler and bottom grab sampler, respectively. Detailed descriptions of the field and laboratory methods used in this study are provided in the following sections.

3.2. Acoustic Doppler Current Profiler (ADCP)

[17] Water column current profiling was performed using a Teledyne RD Instruments (RDI) Workhorse Rio Grande ADCP instrument. Differential Global Positioning System (GPS) data (vessel position and velocity) were integrated using RDI WinRiver II© acquisition software. Horizontal uncertainty for the GPS data, as specified by the manufacturer, was less than 1 m. Both 600 kHz and 1200 kHz ADCP units were used on individual surveys depending on river channel depth. The 1200 kHz instrument used in May 2010 had difficulty accurately resolving the channel bed at higher discharges and in deeper areas of the river. Measurements of water discharge and current velocity were made using the ADCP and standard USGS methodology [*Edwards and Glysson*, 1999] with multiple (2 to 4) cross-channel transects centered over the Myrtle Grove and Magnolia bars (Figure 2). Unresolved instrument error resulted in water discharges measured from the left descending bank to the right descending bank being consistently 10% higher than water discharges measured in the opposite direction. Closer examination of the data reveals this error is the result of higher water velocities measured in one direction rather than different channel cross-sectional areas. For these reasons, all water discharges given in this discussion are the average of measurements made in opposite directions.

[18] The ADCP was operated concurrently with the collection of isokinetic water samples to collect stationary measurements at bar locations at Myrtle Grove, Magnolia, and Alliance. Stationary measurements were carried out for ca. 10–20 min at each location. While these measurements are termed "stationary," safety precautions prohibited anchoring the vessel; rather the vessel maintained an upstream heading and applied sufficient throttle such that the mean vessel velocity (as indicated by vessel GPS) over the duration of measurement was approximately zero. Actual vessel velocities, even under the worst of conditions (e.g., surface waves, heavy wind, and shipping traffic), were less than 0.3 m s^{-1}, and the vessel was at all times within 30 m of the predetermined measurement station. These time-series data were used in the calculation of water column shear velocities and to calibrate the acoustic backscatter to sand concentration. Thousands of vertical profiles of velocity from the stationary measurements were averaged to develop a mean velocity profile at each station, and then an exponential regression was fit to this profile to determine the z_0 value ($z_0 = y$ intercept of the regression function) for the profile. A law of the wall function was constructed according to the equation:

$$u = \frac{u^*}{\kappa} \cdot \ln\left(\frac{z}{z_0}\right), \tag{1}$$

where u is the velocity as a function of height z above the bed, u^* is the shear velocity for the profile, κ is the von Karman constant (0.4), and z_0 is the y intercept value determined above. The value of u^* was adjusted until the law of the wall profile fit the measured velocity profile to determine the average u^* for the measured time period. It was observed that the entire vertical profiles (omitting the lowermost and uppermost several bins) could be reasonably fit to a single law of the wall profile. Therefore, removing either the upper

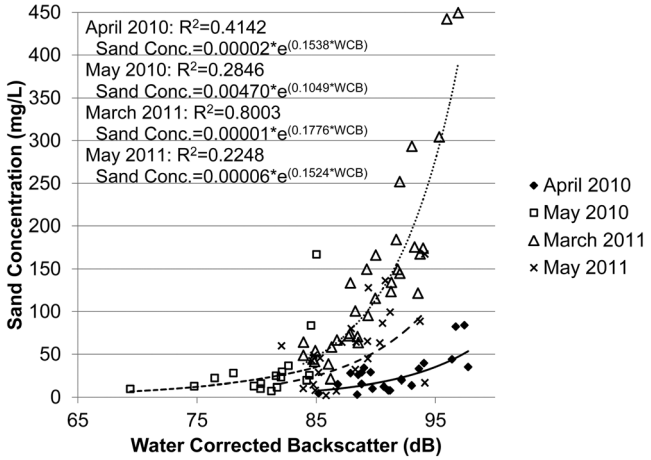

Figure 4. Calibration plot of sand concentration from isokinetic water samples and water-corrected backscatter values measured by ADCP in April 2010 (diamonds), May 2010 (squares), March 2011 (triangles), and May 2011 (cross). Equations for best-fit exponential regression functions for each study period data set are included.

segment or the lower segment (as described by *Kostaschuk et al*. [2004]) did not appreciably change the u^* value of the best-fit profile. The process was repeated using the 30 measured velocity profiles with the highest and lowest standard deviations to estimate characteristically high and low shear velocities for each station.

[19] The u^* values determined above represented the total boundary shear velocity and were therefore corrected for form drag before determining skin-friction shear stress (τ_{sf}). Skin-friction shear stress is the component of total shear stress responsible for the transport of sediment particles [*Kostaschuk et al*., 2004; *Nittrouer et al*., 2011b] and is considered an important parameter to the current study as a fundamental control on sediment transport. First, the shear velocities were converted to total boundary shear stress (τ_b) by the relationship:

$$\tau_b = u^{*2}\rho_w, \tag{2}$$

where ρ_w is the density of water (1000 kg m^{-1}). Next, a ratio of total boundary shear stress to skin-friction shear stress (γ^2) was determined for each measurement by correcting for the size of local bedforms and individual grain roughness according to the relationship of *Nelson and Smith* [1989]:

$$\gamma^2 = \left|\frac{\tau_b}{\tau_{sf}}\right| = 1 + \frac{C_D H_D}{2\kappa^2 \lambda}\left[ln\left(\frac{H_D}{2k_s}\right) - 1\right]^2. \tag{3}$$

[20] Here, C_D represents the coefficient of drag (0.21), H_D the average dune height at that water depth, λ the average dune length, and k_s a grain-size roughness scale equal to the median sand grain diameter found on the bed. Skin-friction shear stress values for each stationary ADCP time series were extracted by dividing the total boundary shear stress by γ^2. This methodology was repeated with the representative high and low shear velocities for each time series to assess the range of skin-friction shear stresses present at each sampling station. While some authors have questioned the reliability of utilizing law of the wall fits for estimation of shear stress [e.g., *Sime et al*., 2007], this methodology was nonetheless employed during the present study because: (1) the length of each time series minimized error induced by turbulent fluctuations in the flow; (2) spatial inconsistencies were minimized by vessel movement between bedform crests and troughs; (3) estimates of skin-friction shear velocity utilizing law of the wall fits compared favorably with estimates utilizing independent methods (e.g., Rouse modeling, bedform transport modeling) in previous studies of the same reach of the Mississippi River [*Nittrouer et al*., 2011b]; and (4) to ensure comparability of the data with that of *Nittrouer et al*. [2011b].

[21] In addition to measurement of water column shear velocities, the stationary ADCP backscatter data were calibrated to measured suspended sand concentrations using the methods outlined by *Topping et al*. [2007]. The first step in this process is the conversion of the 8-bit raw backscatter value (*RB*, measured in counts) recorded by the instrument to the meaningful physical parameter, measured backscatter (*MB*, measured in decibels) by

$$MB = RB \cdot i, \tag{4}$$

where i is the intensity scale factor (in dB count^{-1}) provided by the manufacturer. The measured backscatter value was then corrected for beam spreading and sound absorption by water to the water-corrected backscatter (*WCB*, in dB) utilizing the relationship:

$$WCB = MB + 20\log_{10}R + 2\alpha_w R, \tag{5}$$

where R is the slant range (the along beam distance from the sensor; the beam is oriented 20° from vertical), and α_w is the water absorption coefficient, calculated as

$$\alpha_w = 2.936 \cdot 10^{-5} \cdot \frac{f^2}{f_T}, \tag{6}$$

where f is the sound frequency in kHz and

$$f_T = 2.19 \cdot 10^{\left[6-\left(\frac{1250}{T+273}\right)\right]}, \tag{7}$$

where T is the water temperature in °C. While *Topping et al*. [2007] describe an additional correction for the absorption of sound by fine particles, their method was developed for horizontal backscatter profiles and requires a uniform (or decreasing) concentration along the profile. Vertical profiles in which the sediment concentration increases with distance from the beam cannot be corrected for this additional absorption (since it requires that the relation between *WCB* and *R* has a negative slope). Omission of this correction is unlikely to affect the quality of our calibrations. If it were possible to remove the effect of sound absorption by these particles by adding back what was attenuated (traditionally determined as the negative slope of *WCB* as a function of *R*, which is not the case with our data), it would simply produce an even greater positive slope in our *WCB* vs. *R* profiles, which would enhance only the ability of our method to resolve small differences in sand concentration.

[22] Next, the sediment concentration measured in each isokinetic sample was plotted against *WCB* values measured at the same time and depth (Figure 4). The best correlations were found to be those between *WCB* and sand concentration

(particularly with the March 2011 data, for which isokinetic sampling times were recorded to the nearest second). Data from each study period were fit with exponential regression functions (Figure 4), as the use of different ADCP instruments operating at different frequencies required separate calibrations. These regression functions were then applied to cross-sectional ADCP backscatter measurements to provide cross-sectional profiles of suspended sand concentrations.

3.3. Multibeam Sonar

[23] Bathymetric surveys were conducted with a Reson 7101 swath bathymetry profiler. Attitude data (heave, pitch, roll, and yaw) were collected using an Applanix, Inc. POS/MV gyroscope inertial guidance system. Dual-antenna differential GPS provided position, heading, and velocity data, which were integrated with depth and attitudes at 1 ms intervals. Data were not collected if errors exceeded input thresholds for attitude, heading, position, or velocity (0.05°, 0.1°, 2 m, and 0.5 m s^{-1}, respectively). Vertical resolution for the multibeam instrument, as reported by the manufacturer, is ca. 1.5 cm. CARIS HIPS 7.1© software was utilized for post-processing, including removal of multiples and other noise and navigation drop-outs. Data were then corrected for elevation of the water surface (combined river stage and tidal phase) using hourly USACE water level gage data (www.rivergages.com), referenced to NAVD88 mean sea level at Alliance (Gauge #01390, *RK* 101) for Myrtle Grove data, and at West Pointe a la Hache (Gauge #01400, *RK* 78) for the Magnolia data. Sound velocity profiles derived from conductivity-temperature-depth vertical measurements were applied to the data.

[24] Bedform transport rates were measured on each survey date using a modified version of the survey and post-processing methods developed by *Nittrouer et al*. [2008]. Survey methods were modified to survey only a small bank-to-bank area (ca. 500 m in downstream direction) over the center of each bar, rather than the entire bar area. This was done to reduce the time spent conducting a survey to less than 1.5 h, which minimizes dune migration effects between individual swaths during the survey period. A single bedform transport survey consisted of two bathymetric data sets covering the same area ca. 24 h apart; survey offset was reduced at higher discharges to reflect increased dune celerity. Post-processing methods (after initial corrections to the bathymetric data discussed in the previous section) included defining in ArcMap 10© software polygon sub-areas of the cross-section characterized by similar bedform morphology (i.e., wavelength, height). The number of polygons varied from 3 to 5 for different study sites and time periods, reflecting the dynamic nature of the dunes. Calculated sand volumes (both positive and negative changes in bed elevation) were totaled for each polygon and then an average of the positive and negative change (reflecting both erosion and accretion associated with bedform migration) was utilized. This volume was converted to a mass assuming a sediment porosity of 35% and a grain density of 2650 kg m^{-3}. These quantities were converted to final bed material flux measurements (q_{sb} in $m^2\,s^{-1}$) for each cross-sectional polygon and were then summed cross-channel and converted using sediment grain density to derive a final bedform translational flux (Q_{sb} in T d^{-1}) for that river cross section. See *Nittrouer et al*. [2008] for a more thorough explanation of the equations utilized.

3.4. River Material Sampling

[25] Samples of the riverbed material were collected with a Wildco Shipek Grab sampler in May 2010 at 10 locations each at Myrtle Grove and Magnolia and at seven locations at Alliance (Figure 2). Grab samples from each station were sieved to separate the sand fraction and then the silt/clay (<62.5 μm) fraction was determined by pipette. The sand fraction was analyzed for detailed grain size distribution in a 1.8 m automated settling column in 0.1 phi-size intervals.

[26] One liter volume samples of the water column were collected at three stations along cross sections over the sand bar study areas at Myrtle Grove, Magnolia, and Alliance with a 95 kg, P-63 point-integrated isokinetic water sampler at predetermined depths in the river equaling 30%, 50%, 70%, and 90% of the total water depth [*Edwards and Glysson*, 1999]. The standard method was modified to collect a sample at the water surface rather than at 10% total water depth. The time each sample was collected was recorded for later correlation with acoustic backscatter measurements. Samples were collected at Myrtle Grove and Magnolia in April 2010; on two separate dates at Myrtle Grove and Magnolia in May 2010; in March 2011, two sets were collected at Myrtle Grove, one at Magnolia, and at Alliance; and in May 2011, one set was collected each at Myrtle Grove and Magnolia. While this method neglects the quantity of suspended sediment passing below the 90% water depth interval, it was used nevertheless to maintain compatibility with data from river monitoring stations utilizing depth-integrative samplers (e.g., Belle Chasse; *Allison et al*. [2012]), and no correction has been applied to the unsampled zone.

[27] The concentrations of sand and silt/clay in suspended sediment samples were derived from the isokinetic samples by sieving through a 62.5 μm sieve, and vacuum pumped through 0.4 μm micropore filters to isolate the fine fraction. Isokinetic samples containing a measureable concentration of sand were analyzed for detailed sand grain size using a Retsch Technology CAMSIZER in 0.1 phi-size intervals. Suspended sediment discharges were calculated from the isokinetic sample data and ADCP cross-sectional discharge measurements using the USGS moving-boat method [*Edwards and Glysson*, 1999]. Each river cross section was divided into three subsections, each centered on a vertical sampling location. The depth-averaged sediment concentration (C_s; for both sand and total sediment) for each sampling location was multiplied by the fractional water discharge for that subsection (q_{wn}; determined using the WinRiver II© ADCP software) to determine the sediment discharge for the subsection (q_{sn}):

$$q_{ss_n} = C_s \cdot q_{w_n}, \tag{8}$$

and the subsections were summed to determine the total cross-sectional sediment discharge (Q_s):

$$Q_{ss} = \sum q_{ss_n}. \tag{9}$$

[28] This operation was performed for each of the 2 to 4 repeat ADCP cross sections, and the average was utilized

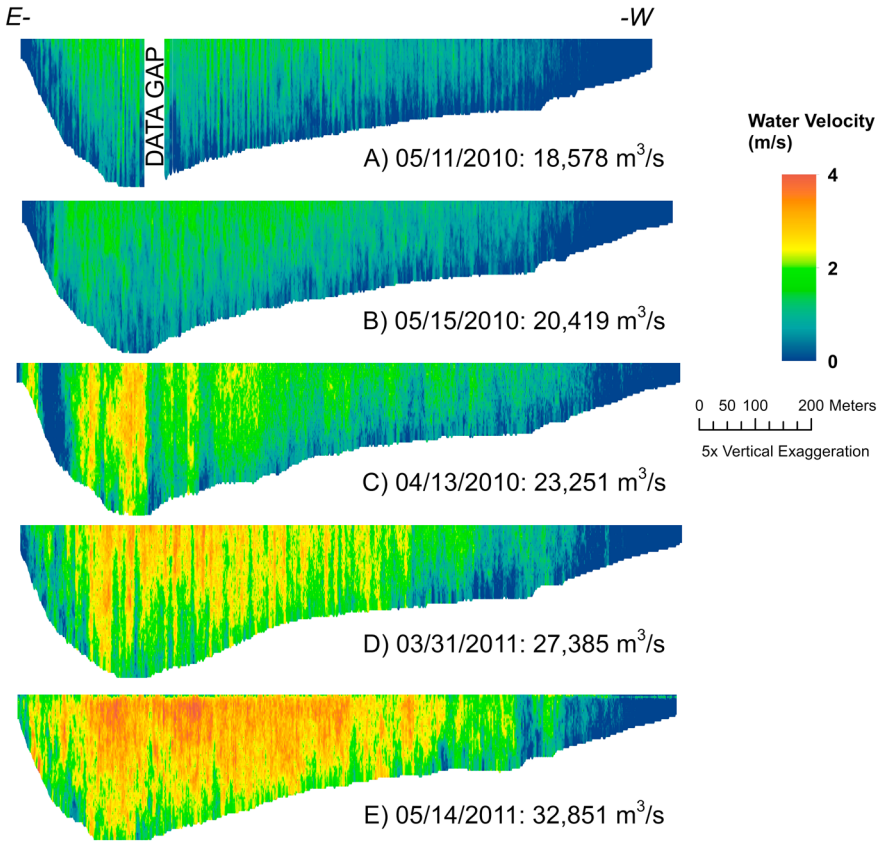

Figure 5. Cross-sectional ADCP measurements of water velocity at Myrtle Grove during each of the study periods. All plots are exaggerated vertically by a factor of five and depict flow into the page. Data gaps occurred where no coherent signal returned to ADCP sensor. Figure 2 displays cross-section location.

for the suspended load flux. While this method does not account for nonlinear increases in sediment concentration within the lowest 10% of the flow, it ensures compatibility of the data with the long-term depth-integrated measurements of the USGS Belle Chasse monitoring station.

4. Results

4.1. Water Discharge and Velocity Characteristics

[29] Water discharges measured by averaging moving-boat ADCP cross-sections at Magnolia, Myrtle Grove, and Alliance during each study period are presented in Figure 3. These values were within error limits of the measured water discharge at the USGS Belle Chasse station. Average water velocities (averaged across the width and depth of the channel) measured at Magnolia ranged from 1.17 m s^{-1} on 11 May 2010 to 2.07 m s^{-1} in May 2011. At Myrtle Grove, average water velocities ranged from 1.27 m s^{-1} in May 2010 to 2.06 m s^{-1} in May 2011. Over the period of stationary-boat velocity data at each station, instantaneous velocities in the upper water column were observed to vary $\pm$1 m s^{-1} about these mean values. Additional variability associated with tidal cycles was observed in velocity records recorded at the USGS Belle Chasse monitoring station; however, the magnitude of this variability (<0.1 m s^{-1}) was less than that of higher frequency river pulses (up to 0.3 m s^{-1}). Cross-sectional measurements of water velocity at Myrtle Grove and Magnolia during each study period are shown in Figures 5 and 6, respectively. These figures illustrate that the highest water velocities occur near the river surface and over the channel thalweg, with decreasing velocities toward the channel bed and banks. With increasing water discharge, the zone of maximum water velocity expands into shallower regions of the flow, and this expansion is more pronounced at Myrtle Grove (Figure 5) than at Magnolia (Figure 6).

[30] Analyses of stationary-boat ADCP time series produced three total shear velocity values: time-averaged, maximum, and minimum (Table 1). All three parameters were observed to increase with total water discharge, in accord with the measured increase in depth-averaged water velocities. Time-averaged total shear velocities increased ca. 10% (from 8–9 cm s^{-1}) over the range of discharges measured, but shear velocity maxima increased by over 30% (15–20 cm s^{-1}).

[31] Skin-friction shear stress values were calculated for each stationary ADCP time series by converting shear velocities to total boundary shear stress and correcting for the form drag effect of dune sizes and bed-particle diameters (Table 1). A set of three values for each time series was calculated using the time-average, maximum, and minimum shear velocities. Figure 7 shows calculated skin-friction shear stress values from all sampling stations and all study periods; skin-friction shear stress values calculated by *Nittrouer et al.* [2011a] for lower and higher discharges in

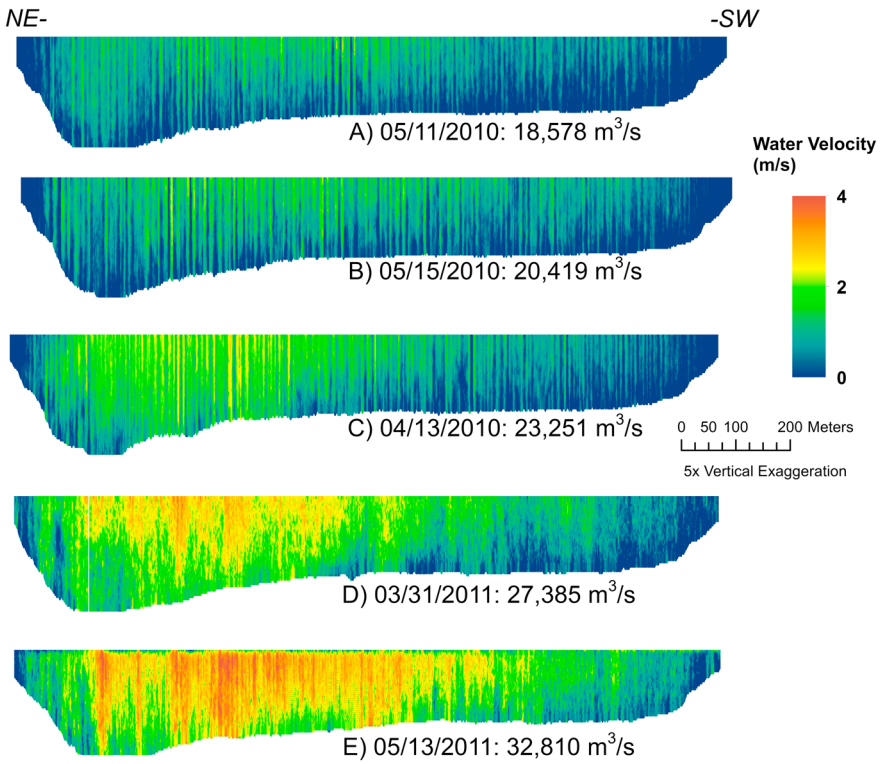

Figure 6. Cross-sectional ADCP measurements of water velocity at Magnolia during each of the study periods. All plots are exaggerated vertically by a factor of five and depict flow into the page. Data gaps occurred where no coherent signal returned to ADCP sensor. Figure 2 displays cross-section location.

the lower Mississippi at Empire, LA (RK 47) are included for comparison. The Empire data collected in 2008 were calculated from moving-boat, rather than stationary, cross-sectional ADCP data. Time-averaged skin-friction shear stress at Myrtle Grove and Magnolia nearly doubled over the range of water discharge between study periods, with substantial increases in maximum and minimum skin-friction shear stress (Figure 7). The variation between minimum and maximum skin-friction shear stress was over an order of magnitude at all measured water discharges, and the least degree of variability was observed during the May 2011 study period. Magnolia exhibited slightly higher values than Myrtle Grove during the April 2010 study period and the higher discharge 2011 study periods. A spatial trend was also noted, where sampling stations at the middle of each sand bar typically exhibited skin-friction shear stresses about 1 Pa less than the deeper and shallower stations.

4.2. River Channel Morphology

[32] Multibeam sonar mapping of the river (Figure 2) at Magnolia, Myrtle Grove, and Alliance reveals that the gently sinuous channel planform is mirrored on the channel floor by thalweg switching from bank to bank. The river cross section is asymmetric between channel crossings, with a steeply sloping bank on the thalweg side. The opposing bank is a gently sloping sand bar covered in dunes of varying size. Dune size statistics (Table 2; wavelengths, heights, aspect ratios) were measured visually from the bathymetric data for general trends and slopes were computed using the first derivative of the channel bed elevation along river-parallel transects intersecting sampling stations 1–3 at Magnolia and Myrtle Grove (Figure 2). In thalweg crossings, the cross section is relatively symmetrical, and the thalweg is often completely covered with sandy alluvium and dunes. In the tight bend segment (low radius of curvature) downstream of Myrtle Grove, the channel bed is devoid of alluvium, and the channel has incised into relict fluvial-deltaic sediments. These segments exhibit erosional sedimentary structures, such as flute casts, striations, and stratal unconformities and escarpments that are outlined in more detail by *Nittrouer et al*. [2011b].

[33] Of the three study areas, the Myrtle Grove reach (Figure 8) is the narrowest (775 m) and has the deepest thalweg (40 m). The dune field on the west bank bar is primarily situated between 15 and 30 m water depths. The westernmost 150 m of the channel bed is a shallow platform feature lacking bedforms, with a sharp escarpment facing the bar top. The largest dunes nearest the thalweg (30–40 m water depth) ranged from 7 m in length and 0.3 m in height during the May 2010 survey to over 100 m in length and 2.3 m in height in March 2011. The smaller dunes closest to the west bank (15–20 m) ranged from 4.5 m long and 0.14 m high to 9 m long and 0.4 m high during the same two study periods. In May 2011, dune sizes (height and wavelength) decreased near the thalweg and increased along the bar top relative to the sizes of dunes in March 2011. During the 2010 study periods (April and May), dune aspect was highest in deep water; in March 2011, aspect was greatest in moderate water depth; and in May 2011, dune aspect was greatest in the shallow areas of the sand bar. These dunes were observed to be nearly symmetrical, with lee slopes only slightly greater than stoss slopes (Table 2),

Table 1. Average, Maximum, and Minimum Total Shear Velocity (u^*) and Skin-Friction Shear Stress (τ_{sf}) Calculated From Stationary ADCP Time Series Depth Profiles[a]

Station	Date	Depth (m)	Average u^* ($m\,s^{-1}$)	High u^*[a] ($m\,s^{-1}$)	Low u^*[a] ($m\,s^{-1}$)	γ^2	Average τ_{sf} (Pa)	High τ_{sf} (Pa)	Low τ_{sf} (Pa)
MAG1	15 Apr 2010	19	0.064	0.148	0.051	2.43	1.69	9.03	1.09
MAG2	15 Apr 2010	20	0.099	0.207	0.083	2.88	3.41	14.90	2.40
MAG4	15 Apr 2010	31	0.099	0.169	0.075	--	--	--	--
MYR1	15 Apr 2010	18	0.075	0.197	0.043	2.85	1.97	13.60	0.66
MYR3	15 Apr 2010	27	0.055	0.189	0.053	3.65	0.83	9.79	0.76
MAG1	11 May 2010	19	0.082	0.125	0.064	--	--	--	--
MAG2	11 May 2010	20	0.099	0.145	0.069	--	--	--	--
MAG3	11 May 2010	23	0.099	0.173	0.067	--	--	--	--
MAG4	11 May 2010	32	0.072	0.108	0.043	--	--	--	--
MYR1	11 May 2010	18	0.065	0.135	0.035	2.23	1.90	8.18	0.55
MYR3	11 May 2010	27	0.072	0.135	0.040	3.26	1.59	5.60	0.49
MAG1	15 May 2010	19	0.068	0.109	0.045	--	--	--	--
MAG2	15 May 2010	20	0.054	0.147	0.054	--	--	--	--
MAG4	15 May 2010	32	0.092	0.144	0.059	--	--	--	--
MYR1	15 May 2010	18	0.073	0.127	0.030	1.84	2.89	8.75	0.49
MYR3	15 May 2010	28	0.098	0.150	0.050	3.02	3.18	7.45	0.83
MYR1	30 Mar 2011	18	0.081	0.171	0.047	2.54	2.58	11.50	0.87
MYR2	30 Mar 2011	21	0.066	0.155	0.061	2.49	1.75	9.66	1.50
MYR3	30 Mar 2011	26	0.080	0.142	0.060	1.94	3.31	10.42	1.86
MAG1	31 Mar 2011	19	0.102	0.197	0.045	2.47	4.21	15.69	0.82
MAG2	31 Mar 2011	20	0.089	0.221	0.064	2.32	3.42	21.07	1.77
MAG3	31-Mar-2011	23	0.088	0.190	0.082	2.27	3.41	15.88	2.96
MYR2	1 Apr 2011	21	0.076	0.182	0.065	2.49	2.32	13.31	1.70
MYR3	1 Apr 2011	27	0.094	0.170	0.072	1.94	4.56	14.93	2.68
MAG1	13 May 2011	20	0.120	0.203	0.087	2.39	6.03	17.26	3.13
MAG2	13 May 2011	21	0.087	0.130	0.069	2.22	3.37	7.61	2.14
MAG3	13 May 2011	21	0.090	0.141	0.078	1.77	4.57	11.21	3.39
MYR1	14 May 2011	19	0.093	0.177	0.076	2.87	3.02	10.93	2.02
MYR2	14 May 2011	21	0.084	0.157	0.081	2.46	2.87	10.01	2.66
MYR3	14 May 2011	28	0.087	0.174	0.074	2.02	3.75	14.99	2.67

[a]The ratio of total boundary shear stress to skin-friction shear stress (γ^2) calculated from equation (3) is included. Stations without skin-friction shear stress values could not be calculated due to a lack of bathymetric data (or a lack of bedforms in the bathymetric data) available for the form drag correction.

and no spatial or temporal trends were observed with changes in dune symmetry. With increasing water discharge, the dune field at Myrtle Grove was observed to expand into shallower areas of the bar that were not active during lower discharge surveys ($18{,}000\,m^3\,s^{-1}$; Figure 9). Note that the methods used to identify bedforms in this study have a horizontal resolution of 1 m; therefore, channel areas that appear to be inactive (no dunes) may actually be covered by bedforms with wavelengths less than 1 m (ripples or small dunes).

[34] The Magnolia reach is relatively shallower, less sinuous in planform, and more symmetrical in cross section than the other study sites, averaging 32 m deep in the thalweg. The bar on the west bank is mantled with dunes ranging in size from 90 m long and 2 m high near the thalweg (25–30 m water depth) to 8 m long and 0.3 m high near the west bank (15–20 m depth), with the largest dunes observed during the March 2011 study period. In May 2011, dune sizes decreased in deep water and increased in shallow water relative to the March 2011 dune sizes. The region of steepest dunes shifted progressively west (toward shallow water) with increasing water discharge. Like at Myrtle Grove, dunes at Magnolia were nearly symmetrical (Table 2), and symmetry did not appear to change significantly over time or space. The dune-covered bar here extends across nearly the entire channel bottom, and the extent of dune covered surface was relatively unchanged between the three mapped study periods (Figure 9). No bathymetry data were collected at Magnolia at lower water discharges; therefore,

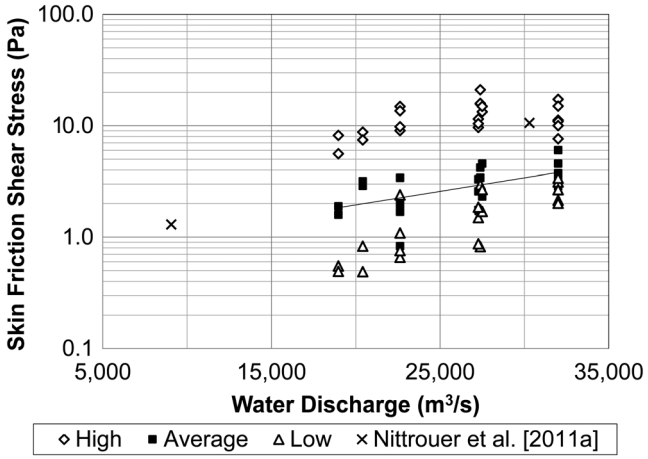

Figure 7. Skin-friction shear stress calculated from stationary ADCP time series data for April 2010, May 2010, March 2011, and May 2011 study periods at Magnolia and Myrtle Grove. Each time series analysis produced three points: a time-averaged shear stress (squares), a highest observed shear stress (diamonds), and a lowest observed shear stress (triangles). Average skin-friction shear stress values calculated by *Nittrouer et al*. [2011a], (cross) in the Mississippi River at Empire, LA (RK 47) are included for comparison. For internal consistency, all water discharge values (including those for the *Nittrouer et al*. [2011a] data) are from the USGS Belle Chasse monitoring station (*Allison et al*. [2012] provide a full discussion of the water discharge data).

Table 2. Dune Geometry Statistics Calculated From First Derivative of Longitudinal (Streamwise) Bathymetry Profiles Centered at Sampling Stations

Station	Date	Depth (m)	Average Stoss Slope	Average Lee Slope	Stoss Slope: Lee Slope	Average Dune Length (m)	Average Dune Height (m)	Dune Aspect Ratio
MYR1	15 Apr 2010	16	0.083	0.078	1.07	4.2	0.17	0.040
MYR2	15 Apr 2010	19	0.105	0.106	1.00	5.1	0.27	0.053
MYR3	15 Apr 2010	25	0.131	0.155	0.84	5.2	0.37	0.071
MAG1	15 Apr 2010	18	0.057	0.065	0.87	5.3	0.16	0.031
MAG2	15 Apr 2010	19	0.096	0.112	0.85	7.0	0.36	0.052
MAG3	15 Apr 2010	22	0.094	0.121	0.78	6.7	0.35	0.053
MYR1	11 May 2010	16	0.048	0.046	1.06	4.2	0.10	0.024
MYR2	11 May 2010	19	0.067	0.067	0.99	4.0	0.13	0.034
MYR3	11 May 2010	25	0.108	0.101	1.07	4.0	0.21	0.052
MYR1	15 May 2010	16	0.029	0.030	0.97	4.3	0.06	0.015
MYR2	15 May 2010	19	0.070	0.081	0.86	6.7	0.25	0.038
MYR3	15 May 2010	25	0.087	0.113	0.77	5.2	0.25	0.049
MYR1	30 Mar 2011	16	0.071	0.082	0.87	7.6	0.29	0.038
MYR2	30 Mar 2011	19	0.083	0.090	0.92	11.4	0.49	0.043
MYR3	30 Mar 2011	25	0.049	0.064	0.78	13.6	0.38	0.028
MAG1	31 Mar 2011	17	0.062	0.074	0.84	6.5	0.22	0.034
MAG2	31 Mar 2011	19	0.066	0.080	0.82	9.9	0.36	0.036
MAG3	31 Mar 2011	22	0.064	0.074	0.87	8.3	0.28	0.034
MAG1	13 May 2011	17	0.063	0.068	0.93	7.4	0.24	0.033
MAG2	13 May 2011	19	0.056	0.081	0.69	10.3	0.34	0.033
MAG3	13 May 2011	22	0.040	0.044	0.91	14.1	0.30	0.021
MYR1	14 May 2011	17	0.095	0.120	0.79	9.1	0.48	0.053
MYR2	14 May 2011	20	0.071	0.090	0.79	9.8	0.39	0.040
MYR3	14 May 2011	25	0.048	0.055	0.87	7.9	0.20	0.026

the transition from lower plane bed to dune formation was not observed there.

[35] Spatial and temporal trends were observed in the evolution of dune geometries at Myrtle Grove and Magnolia (Figure 10; constructed by analyzing longitudinal dune profiles for average geometries at three locations each at Myrtle Grove and Magnolia). The location of maximum dune aspect shifted from deep water (20–25 m) at low discharges (18,000–23,000 $m^3 s^{-1}$) to shallow water (15–20 m; 27,000–31,000 $m^3 s^{-1}$) at higher discharges. It appears that the location of maximum dune aspect in the cross-channel direction is associated with the shallow limit of dune formation noted above in Figure 9, suggesting that high aspect ratios are associated with growing dunes.

[36] The Alliance reach has a highly asymmetrical cross section (30 m deep thalweg) similar to that of the Myrtle Grove reach; however, as at Magnolia, there is limited exposure of relict substrate, except along steep bank areas. A unique feature of the sand bar at Alliance is an elongate, trough-shaped structure parallel to the channel, evidence of a sand-mining operation (CWPPRA Bayou Dupont Sand Mining for Coastal Restoration) completed in March 2010—prior to the initial survey in May 2010 (Figure 2a). Repeat multibeam bathymetric surveys of the Alliance reach in the present study indicate the bar adjusted to the loss of material by aggradation inside the excavated zone, especially at the upstream end, and erosion of the sharp escarpments surrounding and downstream of the feature. The total amount of bed material that had infilled the trough between surveys was calculated as 59,711 T between May 2010 and March 2011, and 281,505 T between March 2011 and May 2011 (assuming 35% porosity and 2.65 g cm^{-3} grain density).

4.3. Bed Granulometry

[37] All bed samples collected in May 2010 had mean and median grain sizes in the range of 150–350 μm, and the mean grain size of all samples was 225 μm, with a tenth percentile grain diameter of 176 μm and a ninetieth percentile grain diameter of 303 μm. There is a slight trend toward finer mean grain sizes with increasing sample water depth at the main sampling transects (Figures 2b and 2c). No samples were collected from relict fluvial-deltaic substrate areas exposed on the thalweg and along steep channel walls.

4.4. Suspended Sediment Loads Derived From Isokinetic Data

[38] Concentrations of silt and clay in isokinetic water samples were relatively depth-homogeneous during all study periods (Figure 11). Suspended silt and clay load ranged from 150,000 T d^{-1} in April 2010 to over 500,000 T d^{-1} on 11 May 2010, but decreased to 300,000 T d^{-1} by 15 May 2010 (Table 3 and Figure 12). Suspended silt and clay loads in March and May 2011 were intermediate—about 300,000 T d^{-1}. It is apparent from these data that the silt and clay load does not correlate with water discharge; the highest load was measured on the date with the lowest water discharge (11 May 2010) and was similar on 15 May 2010 and March 2011 in spite of a substantial difference in water discharge (ca. 35% increase). No correlation between silt and clay load and study reach was observed.

[39] Sand concentrations from the isokinetic water samples increased nonlinearly with proximity to the bed (Figure 11). Suspended sand loads ranged from less than 20,000 T d^{-1} on 11 May 2010 to about 200,000 T d^{-1} in March 2011, with intermediate values during April 2010 and May 2011 of about 45,000 T d^{-1} and 130,000 T d^{-1}, respectively (Figure 12). The contribution of sand to total suspended sediment load ranged from less than 10% in May 2010 to about 40% in March 2011. No correlation between sand load and study reach was observed from the data calculated using isokinetic sample concentrations.

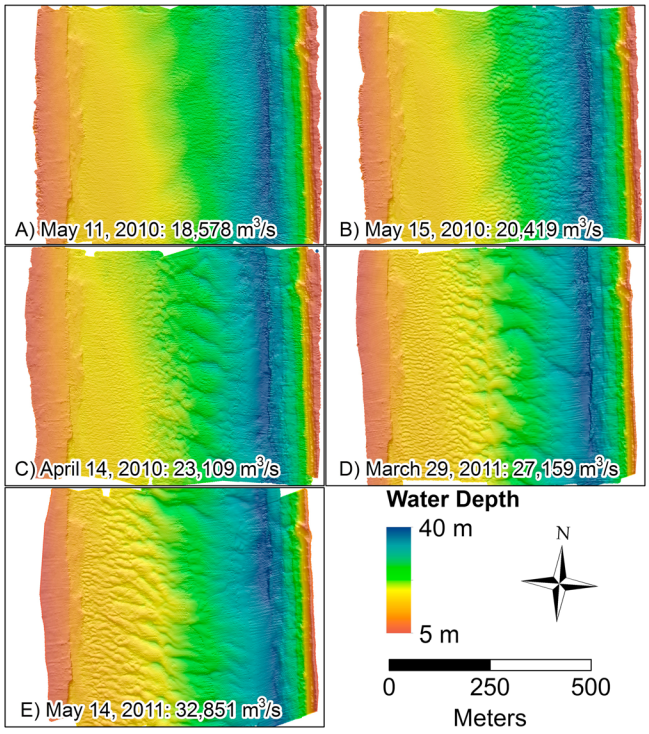

Figure 8. Multibeam sonar bathymetry of the Myrtle Grove bedform transport study grid at five different dates reflecting variable nature of sand bar bedforms. Water discharge is daily averaged at the nearby USGS Belle Chasse monitoring station. Figure 2 displays the location of the bedform survey grid.

[40] Detailed CAMSIZER grain-size analysis indicates that the suspended sand fractions in most samples are normally distributed (Gaussian), with occasional bimodal distributions and coarse skewness. There is a general trend of gradual coarsening of the sand population from surface to 0.9 water depth. In general, shallow water samples contained sand populations with a mode near 125 μm, and near-bed samples had modal grain sizes in excess of 250 μm. This relation is shown best in the data from March 2011, when surface samples contained measurable quantities of sand and samples were collected from all five fractional water depths. The fraction of sand greater than 176 μm serves as an indicator of sizes equivalent to bed material (e.g., bed material load in suspension). These show similar trends to total sand concentrations. Samples collected in 2010 contained nearly negligible amounts of sand greater than 176 μm except near the bed; however, samples from the higher water discharge studies in March and May 2011 contained substantially higher concentrations of this size fraction, with measurable amounts even found in surface water samples. The fractional contribution of sediment larger than 176 μm to total suspended loads was generally observed to increase with water discharge, being less than 10% (averaged between Myrtle Grove and Magnolia) in May 2010, rising to 23% in March 2011, and falling slightly to 19% in May 2011.

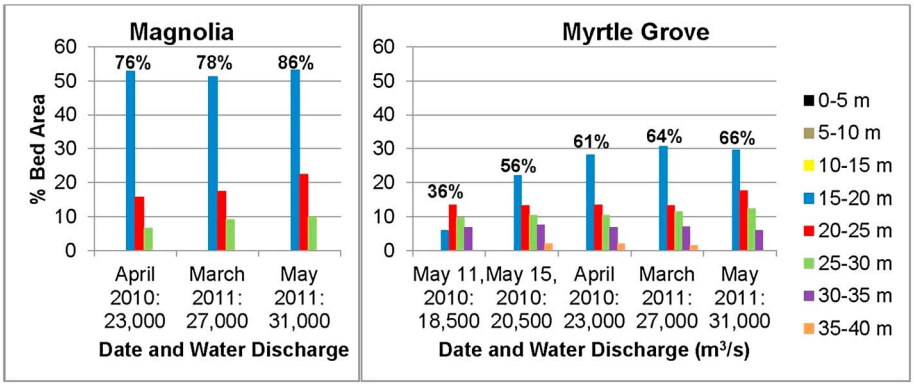

Figure 9. Extent of surveyed channel area (within bedform grids; Figure 2) covered by bedforms at Magnolia and Myrtle Grove, for five study periods. Individual bars represent percentage of total channel area covered by dunes at 5 m water-depth intervals. Percentages above each group indicate total channel-bed area covered by bedform.

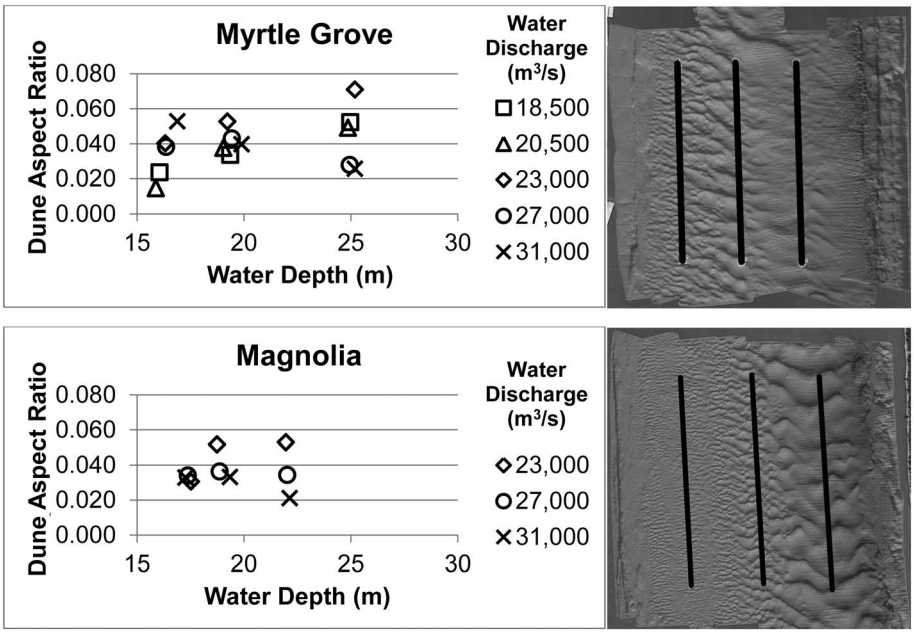

Figure 10. Bedform aspect ratios (height/wavelength) for measured dune profiles at Myrtle Grove and Magnolia as a function of water depth and water discharge (study period). Locations of the longitudinal dune profiles used for aspect ratio calculation are provided for each study site.

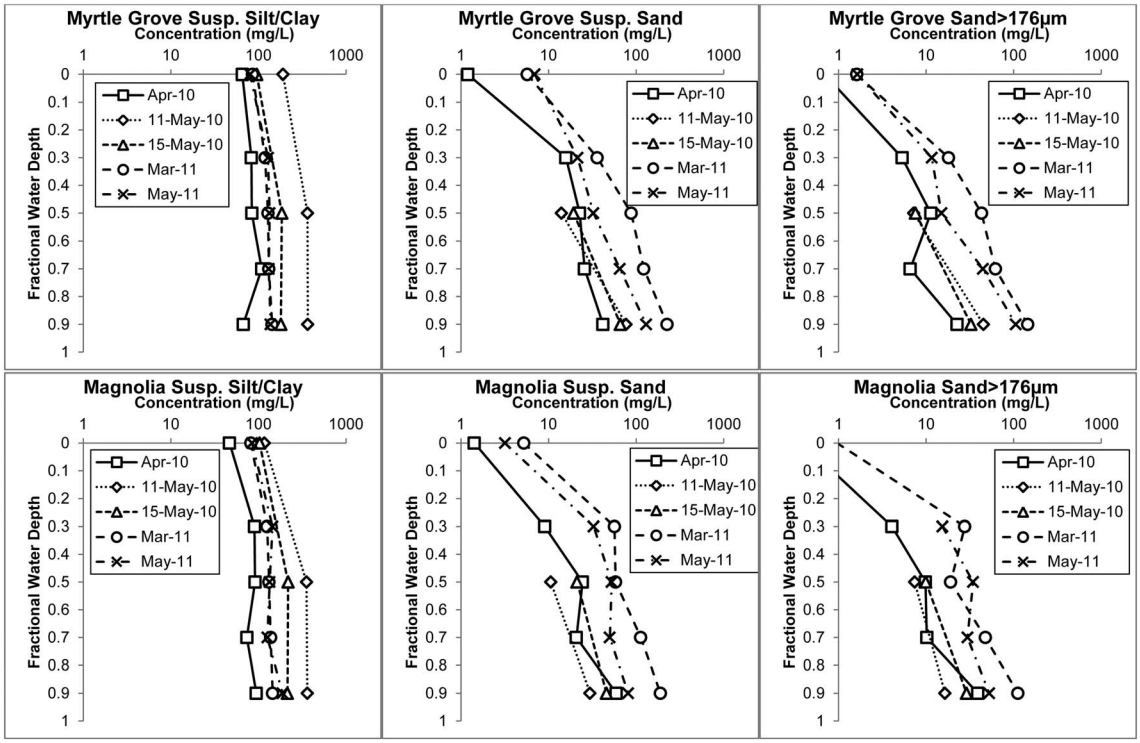

Figure 11. Summary of suspended sediment concentrations measured in isokinetic water samples for each of the study periods (April 2010, 11 May 2010, 15 May 2010, March 2011, and May 2011) for Myrtle Grove (top row) and Magnolia (bottom row). Left to right at both sites are plotted silt/clay concentration, total sand concentration, and bed material sand (>176 µm) concentration. Each vertical profile in this figure was constructed by calculating the average concentration for each depth fraction at the four sampling stations at the Myrtle Grove and Magnolia study areas (i.e., cross-channel averaged sediment concentrations).

Table 3. Cross-Sectional Water Discharge, Suspended Silt/Clay Discharge, Suspended Sand Discharge (Calculated Using Both Isokinetic Water Samples and ADCP Backscatter Cross Sections at Myrtle Grove and Magnolia), and Percent Contribution of Sediment Larger Than 176 μm Diameter (i.e., Bed Material) to Total Suspended Discharge

Site	Date	Water Disch. (m^3/s)	Water Disch. Stand. Dev.	Susp. Silt/Clay (Tons/Day)	Silt/Clay Stand. Dev.	Susp. Sand (Tons/ Day)	Sand Stand. Dev.	ADCP Susp. Sand (Tons/Day)	% Larger Than 176 μm
Magnolia	15 Apr 2010	22,429	792	154,364	5338	44,890	1480	70,590	12.5
Myrtle Grove	15 Apr 2010	23,281	859	166,851	6855	44,597	1483	56,350	10.6
Myrtle Grove	11 May 2010	18,770	459	500,229	11,929	49,502	878	34,645	5.2
Magnolia	11 May 2010	19,343	1233	468,051	29,534	19,209	1503	40,479	2.8
Myrtle Grove	15 May 2010	20,573	893	274,062	11,867	49,531	1559	48,693	7.1
Magnolia	15 May 2010	20,673	1245	321,127	19,010	41,558	2189	48,836	10.9
Myrtle Grove	30 Mar 2011	27,097	1379	293,830	15,276	190,874	10,901	141,530	23.1
Magnolia	31 Mar 2011	27,364	1360	302,111	14,707	199,533	9346	145,606	22.0
Magnolia	13 May 2011	31,493	1015	367,707	11,599	111,917	4455	99,056	15.6
Myrtle Grove	14 May 2011	32,138	965	343,249	10,231	154,954	4620	98,465	21.9

4.5. Suspended Sand Load From Calibrated ADCP Backscatter Measurements

[41] In Figures 13 and 14, cross-sectional ADCP backscatter transects were processed using the calibration relations developed between isokinetic suspended sand concentration data and water-corrected acoustic backscatter for each study period (Figure 4) to construct cross-sectional profiles of suspended sand concentrations at Myrtle Grove and Magnolia, respectively. These cross sections have been grouped by increasing water discharge (i.e., the same cross-section measured at five different times) to examine the variation of suspended sand concentrations at each reach. An important caveat for these calibrated ADCP data is that the May 2010 profiles were measured using a 1200 kHz instrument; and April 2010, March 2011, and May 2011 profiles were made with a 600 kHz ADCP. The different frequency instruments were calibrated separately (Figure 4), owing to a frequency-dependent relation between fluid sound absorption and beam range, and a much closer relation was observed between 600 kHz backscatter and suspended sand concentration in April 2010, March 2011, and May 2011 than between 1200 kHz backscatter and sand concentration in May 2010. Several artifacts exist in the 1200 kHz data that are not observed in the 600 kHz data, such as a tendency for the beam to be unable to resolve the riverbed in deeper and/or more turbulent water and a tendency toward unusually high backscatter values measured near the surface, even after calibration for sound energy losses. It should also be noted that these data do not represent instantaneous measurements of suspended sand concentrations; the ADCP collected data as the survey vessel traveled across the channel at 1–2 m sec^{-1}; a full transect required 5–10 min. Sand loads calculated from the calibrated ADCP backscatter cross sections (Table 3) were comparable to those calculated using the isokinetic method, but the backscatter-measured sand loads were always higher (up to 20%) for Magnolia than for Myrtle Grove. Suspended sand loads calculated by both methods correlated directly with water discharge (Figure 12). The regression function shown for USGS Belle Chasse isokinetic data suggests that there is negligible suspended sand at water discharges below about 10,000 $m^3 s^{-1}$.

[42] At the lowest measured water discharge, sand concentrations higher than 50 mg L^{-1} were not measured in the water column at Myrtle Grove (Figure 13a; 18,578 $m^3 s^{-1}$). With increasing discharge, the zone of maximum sand concentration increased in extent and concentration to a maximum in March 2011 (Figure 13d; 27,385 $m^3 s^{-1}$) when suspended sand was observed over the entire bar, reaching concentrations greater than 250 mg L^{-1} on the central bar top. At the highest discharge (Figure 13e; 32,851 $m^3 s^{-1}$), suspended sand was still observed over the entire bar at Myrtle Grove but the zone of high near bed concentrations was reduced in extent and maximum concentration, with less sand observed in suspension near the thalweg and over deeper areas of the sand bar (Figure 13e). The Magnolia reach displayed a similar trend of increasing suspended sand concentrations with increasing water discharge between May 2010 (Figure 14a) and March 2011 (Figure 14d), and a decrease in suspended sand concentration in May 2011 (Figure 14e). However, little variation with water discharge was observed in the lateral extent of

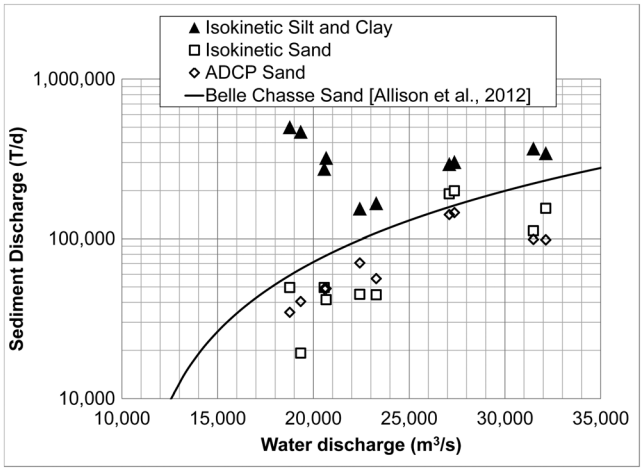

Figure 12. Calculated suspended silt/clay and sand discharge plotted against water discharge: each point represents a single average for a study reach (Magnolia or Myrtle Grove) and study period in 2010–2011. Diamonds calculated from ADCP backscatter cross sections, triangles, and squares are calculated by integrating isokinetic sample concentrations with cross-sectional ADCP water discharge measurements, black line is regression function fit to 3 years (2008–2010) of USGS isokinetic suspended sand discharge data from Belle Chasse, LA [*Allison et al*., 2012].

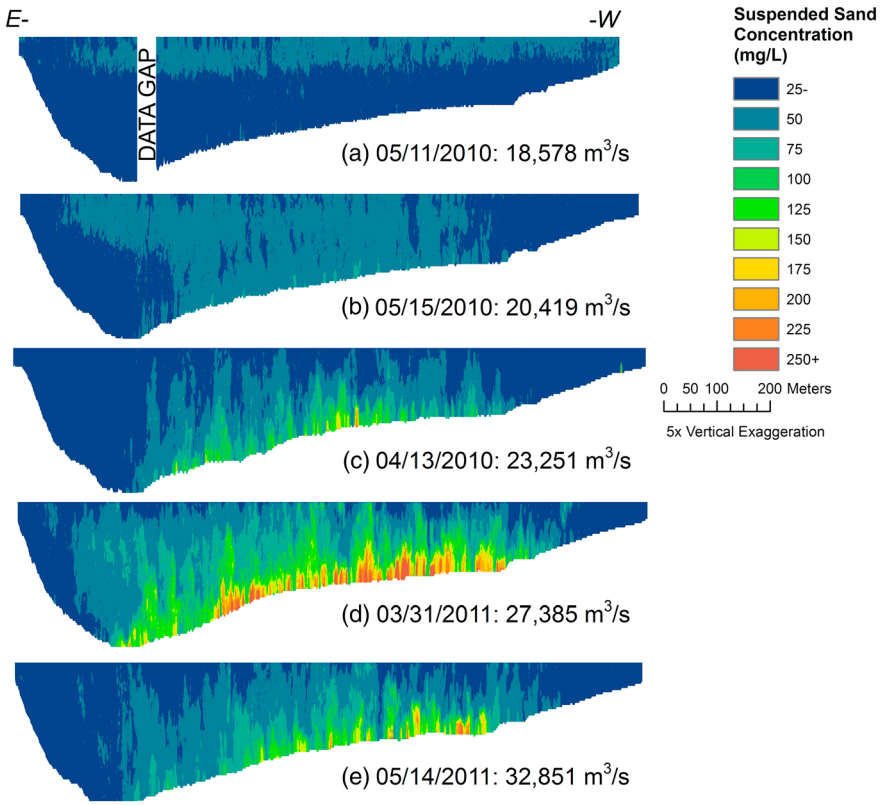

Figure 13. (a–e) Calibrated cross-sectional suspended sand concentrations from ADCP backscatter measurements at Myrtle Grove over a range of water discharge conditions (water discharge from USGS Belle Chasse monitoring station tidally-averaged daily values). All plots are exaggerated vertically by a factor of five, and depict flow into the page. Data gaps occurred where no coherent signal returned to ADCP sensor. Figure 2 displays cross-section location.

near-bed suspended sand concentration at Magnolia, except perhaps during the lowest discharge survey (Figure 14a; 18,578 $m^3 s^{-1}$), when near-bed sand activity was restricted to 20–25 m water depths.

4.6. Bedform Transport Rates

[43] Calculated bedform transport rates on the sand bars at Myrtle Grove and Magnolia are summarized in Figure 15 and Table 4 relative to daily averaged river discharge measured at Belle Chasse monitoring station. No surveys of bedform transport were made at Alliance. Bedform transport rates were exponentially related to water discharge for observations from both sites made in April 2010, March 2011, and May 2011. Channel bed areas with the largest dunes exhibited the highest rates of daily bedform flux. Bedform transport rates calculated in May 2010 for the Myrtle Grove site fell well below the exponential best-fit regression line (Figure 15). No statistically significant difference was observed when comparing relative rates of bedform accretion and erosion between study sites.

5. Discussion

5.1. Differentiating Local Versus Non-Local Sand in Suspension

[44] The observed complex relation between suspended sediment discharge and water discharge is associated with the concept of wash load and bed material load in rivers. As outlined in section 2.1, *wash load* refers to finer grains not present in the channel bed, and is transported in suspension, while *bed material load* is the alluvial component of the channel bed, typically sand-size and larger, which may be transported as bedload (traction) or in suspension [*Gomez et al.*, 1989; *Gomez*, 1991; *Church*, 2006]. The term *bed material* does not imply a transport mode, only the source of material; therefore, the terms *suspended bed material* and *bed material in traction* will be used here to denote transport mode, and *bed material load* will refer to the combined quantities that constitute the total downstream transport of sand-sized material that originates in the bed.

[45] The sand particles larger than 176 μm are defined as bed material because these are the principal grains sizes measured in channel-bed grab samples (the tenth percentile grain size found in the channel bed is 176 μm). These particles may be considered locally sourced. Note that the term "local" used here is relative to the time frame of interest. For the several-day study periods of the present investigation, bed material in traction may be considered local to a particular sand bar, because individual bedforms were able to be tracked over several days of migration. For bed material in suspension transport, a first-order approximation of minimum (i.e., assuming no ongoing turbulent suspension processes after an initial resuspension event) downstream excursion lengths of individual particles may be estimated using the settling velocities [*Gibbs et al.*, 1971] for the range of grain sizes present in the channel bed. Considering a grain

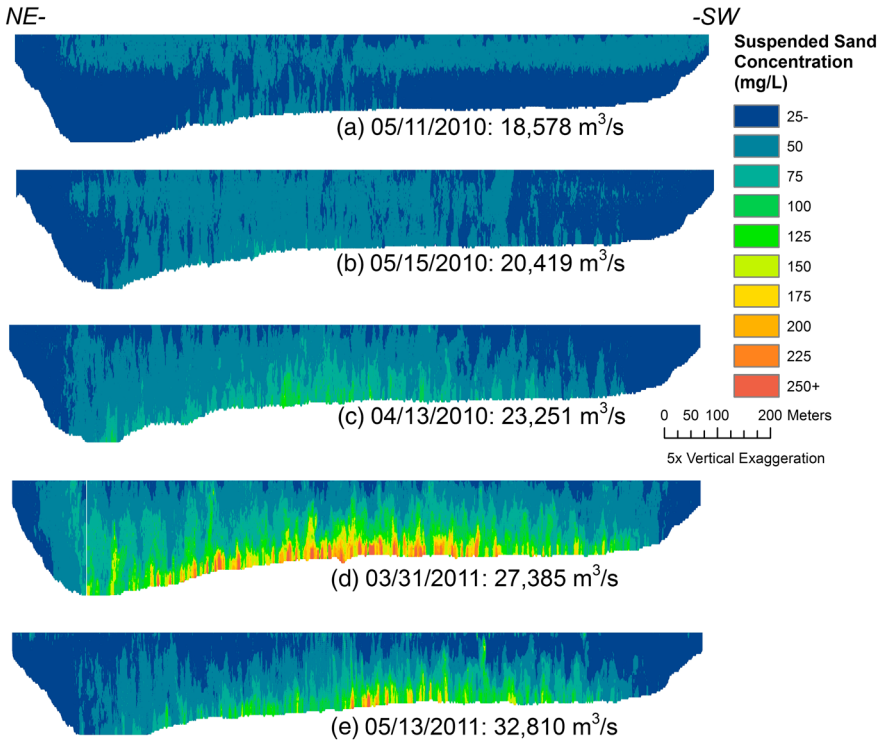

Figure 14. (a–e) Calibrated cross-sectional suspended sand concentrations from ADCP backscatter measurements at Magnolia over a range of water discharge conditions (water discharge from USGS Belle Chasse monitoring station tidally-averaged daily values). All plots are exaggerated vertically by a factor of five, and depict flow into the page. Figure 2 displays cross-section location.

suspended up to 0.5 total water depth (~10 m for typical water depths over the bars at Myrtle Grove and Magnolia) and a depth-averaged water velocity of 1.5 m s^{-1}, excursion lengths for a single suspension event may range from 345 m (303 μm sand) to 724 m (176 μm sand). Individual grains may be deposited after a suspension event and resume traction transport at rates generally less than a dune wavelength per day, or grains may be subjected to many consecutive suspension events and travel 10 s of km in 1 day. Therefore, when considering suspension transport, the concept of a local sediment source may extend several sand bars upstream.

[46] For the discharges observed during the present study, silt/clay and sand smaller than 176 μm may be considered wash load because these particle sizes are not found in appreciable quantities in the channel bed. Because these particles are not deposited in this reach, their source is not local, and their supply is not related to flow conditions in the river itself. This is supported by the daily total sediment load record over the study period from calibrated optical backscatterance sensor (OBS) data at the USGS Belle Chasse station (Figure 3, dashed line; *Allison et al.* [2012]), which indicates that total suspended sediment load peaks early during water discharge peaks, and our results (Figure 12) confirm that silt, clay, and fine sand (<176 μm) are the majority of the total suspended load. The early sediment peak is attributable to drainage basin runoff (i.e., fine sediment) that is largely exhausted before peak water discharge, a hysteresis effect that has been widely documented in the Mississippi River [*Mossa*, 1996; *Galler and Allison*, 2008; *Allison et al.*, 2012]. During the brief (days-to-weeks) period when fines stored in-channel at water depths less than ca. 20 m at low discharges are remobilized during rising discharge, these fines can technically be considered a bed material contribution to sediment discharge [*Demas and Curwick*, 1987; *Galler and Allison*, 2008].

5.2. Effect of Flow Conditions and Dune Morphology Controls on Bed Material Resuspension

[47] The evolution of flow conditions and the morphology of sand bar surfaces at Myrtle Grove and Magnolia with increasing water discharge may help explain the spatial and temporal patterns of suspended sand concentration observed during the study periods. If the skin-friction component of the total bed shear stress is responsible for the actual movement of bed material grains, then examination of the relations between skin-friction shear stress and water discharge may elucidate the complex relations between water discharge, dune morphology, and bed material transport. At all measured water discharges, estimates of time-averaged skin-friction shear stress (Figure 7) were well above the threshold shear stresses for grain movement and significant suspension (0.73 Pa for the median grain size of 225 μm; *Bagnold* [1966]). The evolution of the channel bedforms with increasing shear stress during this study follows the trend recognized in previous studies of alluvial streams (e.g., *Yalin and Karahan* [1979]; *Fredsøe* [1982]; *Schreider and Amsler* [1992]), in which dune aspect increases with excess shear stress to a point, and then decreases as increasing shear stress leads to increased suspension transport and dune washout, as observed at the Myrtle Grove reach in May 2011. This high excess skin-friction shear stress also explains the presence of suspended bed material at

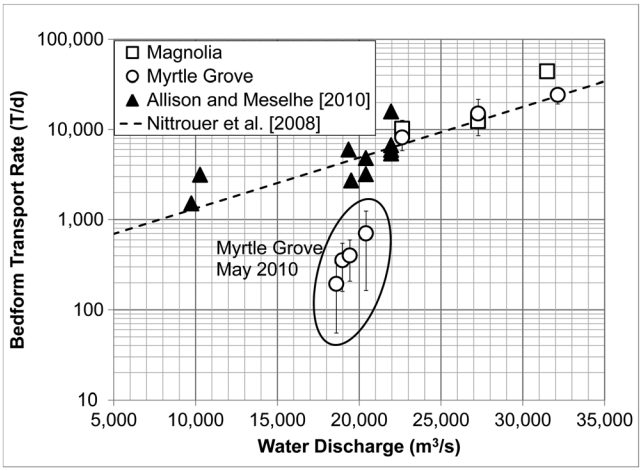

Figure 15. Calculated bedform transport rates at Magnolia and Myrtle Grove (white squares and white circles, respectively) as a function of daily-averaged water discharge at the USGS Belle Chasse station. Black triangles are data from Magnolia, Myrtle Grove, and the third site at Empire, LA (RK 47) measured in 2008 and 2009 by *Allison and Meselhe* [2010]. The exponential regression function from *Nittrouer et al*. [2008] is included for comparison. Measurements from Myrtle Grove in May 2010 (circled) fell well below predicted values for this reach of the river.

all measured discharges. Given the wide variability in skin-friction shear stress observed during each study period, however, minimum estimates of skin friction varied about the threshold for full suspension during the study periods in April and May 2010 (Figure 7), perhaps due to periodic dune-induced turbulent fluctuation [*Lapointe*, 1992; *Bennett and Best*, 1995]. This suggests resuspension events may have been intermittent at these water discharges, leading to lower concentrations of suspended bed material (Figures 11, 13, and 14). As water discharge increased over 25,000 $m^3 s^{-1}$ during the March and May 2011 study periods, skin friction estimates were at all times above the threshold value (Figure 7), and bed material entrainment may have been more continuous, resulting in higher suspended concentrations (Figure 11). Additionally, the growth of dunes into shallower areas of the bar during the high discharge surveys (Figures 8 and 9) increased channel-bed roughness in these areas (steeper dunes; Figure 10), which may have led to greater turbulence intensity there and increased suspension of bed material, particularly at Myrtle Grove (Figures 13d and 13e). As discharge rose even higher between March and May 2011, suspended sand concentrations decreased in deeper areas of the bar at Myrtle Grove, likely as the result of dune washout there (Figure 8), which has the compounding effects of decreasing the availability of sand and attenuating turbulent fluctuations (due to flattening of the bed; Figure 10). It is unclear which of these mechanisms (if not both) was most responsible for the decrease in bed resuspension in this area; however, *Allison et al*. [2013] describe a trend of increased mean grain size of the channel bed from low to high discharge in the vicinity of the Bonnet Carré as a result of removal by suspension of the finer bed fraction, which could lead to a less-easily resuspended bed. Nevertheless, the increased suspension of bed material in shallow bar areas and the decreased suspension in deep bar areas at Myrtle Grove led to an apparent shallowing of the zone of maximum sand suspension (Figure 13), and therefore a lateral shift in bed material transport.

[48] The observations of infilling at the Alliance reach between study periods may also support the notion of a laterally mobile zone (i.e., migrating cross-river) of bed material transport. The rate of infilling between the May 2010 and March 2011 study periods (188 T d^{-1}; 59,711 T of material deposited over 318 days) was nearly an order of magnitude less than that, which would be predicted for the average discharge during that period by bedform transport measurements made in other studies of the below-New Orleans reach of the river (over 1000 T d^{-1}; *Nittrouer et al*. [2008]; *Allison and Meselhe* [2010]). If the active zone of bed material transport shifts from deep to shallow areas of the bar between low and high water discharge, then it can be anticipated that the majority of bed material transport during the low discharge May 2010 to March 2011 period would be restricted to higher-energy areas along the deeper bar face, at depths below the dredged cut. On the other hand, at higher water discharges (such as during the March 2011 to May 2011 interval), this hypothesis would predict greater bedload transport rates and enhanced bed material transport in shallower areas of the sand bar. The hypothesis is supported by the filling rate of over 6000 T d^{-1} (281,505 T of material deposited over 43 days) in the dredge area, which is close to the bedload transport rate predicted by the regression function of *Nittrouer et al*. [2008], and indicates that substantial quantities of bed material are being transported in shallow areas of the bar at Alliance during high discharge. Additional support for our hypothesis comes from examination of the hydrograph of the river prior to our initial surveys at Myrtle Grove (the period during which the dredging took place). In the months preceding May 2010, several large flood peaks occurred, all in excess of 25,000 $m^3 s^{-1}$. Each of these floods would have been energetic enough (given our observations during this study) to shift the main area of bed material transport into shallow areas of the sand bar at Alliance, where the area of ongoing dredging would have been trapping bed material and preventing it from being transported downstream to Myrtle Grove. The removal of this upstream source of bed material could also help explain the lower-than-predicted rates of bedform transport measured at Myrtle Grove in May 2010.

5.3. Implications for Environmental Restoration

[49] The results of this study are relevant to ongoing and planned coastal restoration efforts both in the Mississippi River delta and around the world. A number of large river diversions have been proposed for the lower Mississippi River, with the primary purpose of delivering river sediment to build land in coastal areas [*LACPRA*, 2012]. Recent studies have documented the opening of the Bonnet Carré flood control spillway in May 2011 and examined the effects both within the Mississippi River channel [*Allison et al*., 2013] and in the spillway itself [*Nittrouer et al*., 2012]. *Allison et al*. [2013] concluded that the opening of the spillway and removal of 20% of Mississippi River water during a peak flood caused a reduction in the sediment transport capacity of the river, leading to the deposition of suspended sand downstream of the spillway and substantial shoaling in the channel. They noted that channel shoaling is a problem for the navigation industry which must maintain a channel for deep draft vessels.

Table 4. Calculated Bedform Transport Rates for Magnolia and Myrtle Grove in April 2010, May 2010, March 2011, and May 2011[a]

Location	Date	Bedform Transport (Tons/Day Accreted)	Bedform Transport (Tons/Day Eroded)	Average Bedform Transport (Tons/Day)	Water Discharge (m^3/s)	Erosion: Accretion
Magnolia	15 Apr 2010	11,952	8,498	10,225	22,628	0.71
Myrtle Grove	15 Apr 2010	6,514	9,830	8,172	22,628	1.51
Myrtle Grove	12 May 2010	96	293	194	18,606	3.05
Myrtle Grove	13 May 2010	493	217	355	18,974	0.44
Myrtle Grove	14 May 2010	540	265	402	19,428	0.49
Myrtle Grove	15 May 2010	1,085	322	703	20,419	0.30
Magnolia	30 Mar 2011	11,469	13,338	12,403	27,272	1.16
Myrtle Grove	30 Mar 2011	19,716	10,472	15,094	27,272	0.53
Magnolia	13 May 2011	44,197	44,032	44,115	31,493	0.99
Myrtle Grove	14 May 2011	20,726	27,849	24,288	32,138	1.34

[a]Accreted bed material is calculated from the volume of sediment deposited on the lee side of bedforms, and eroded bed material is calculated from the volume of sediment eroded on the stoss side of bedforms. Water discharge referenced to Belle Chasse monitoring station value during the second day of each bedform transport survey. Erosion:accretion >1 signifies deflation (net loss of material) of the sand bar.

Nittrouer et al. [2012] documented a large deposit of sand within the spillway and suggested that future river diversions can be designed to disperse captured sand to build land. These results indicate that the optimal design and operation of land-building diversions should minimize the capture of water (to prevent shoaling in the channel associated with the loss of stream power) while maximizing the capture rate of sand, and both these studies and others (e.g., *Allison and Meselhe* [2010]) suggest that engineered diversions can do so by tapping into the high suspended sand concentrations near the channel bed.

[50] The results of the present study highlight the existence of two distinct sources of sand in the tidal reach of the Mississippi River: a drainage basin (wash load) component and a local (bed material) component that comprise the total sand load of the river. While bed material sand makes up less than 25% of the total suspended load (even at high discharge), it is the majority of the suspended sand load. Diversions seeking to maximize the capture of sand must take into account the differing transport pathways for these components. Quantities of wash load are largely a function of drainage basin supply issues, rather than flow conditions in the tidal reach, particularly during high discharge when the backwater effect of decreasing water surface slopes is at a minimum [*Nittrouer et al*., 2011a]. Capture of this material may be maximized by examination of up-to-date monitoring station data (e.g., OBS turbidity records; Figure 3) to open diversions during the brief peaks of high wash load. These peaks have been demonstrated to coincide with the rising limbs of individual (weeks to months) flood events as well as summer contributions from the Missouri River tributary [*Allison et al*., 2012]. Perhaps the most important feature of wash load is the silt and clay component, which is at all times the majority of the river's sediment load. This component cannot be neglected from estimates of sediment capture by diversions and it may comprise the major fraction of any deposits created by these diversions. The contribution of silt and clay to land-building efforts may be maximized by citing diversion receiving basins in low energy environments, where these sediments will be less easily eroded.

[51] Bed material loads on the other hand show a strong dependence on the water discharge and the flow conditions of the river (Figures 12 and 15). Rates of capture for this material may be enhanced by operating diversions at high water discharges to coincide with the nonlinear increases in sand transport conditions (e.g., bedform migration rates, *Nittrouer et al*. [2008]; skin-friction shear stress, *Nittrouer et al*. [2011b]; and total sand loads, *Allison et al*. [2012]). Because this material is sourced locally from discrete sand bars, capturing too much or operating several diversions in close proximity may lead to depletion of the source. However, the infilling rates of the dredged area at Alliance (sections 4.2 and 5.2) indicate that substantial quantities of bed material may be renewable over short (several years) time scales relative to the operational life of proposed diversion projects (decades–centuries; *LACPRA* [2012]). The renewal of this dredged material also suggests that the efficiency of sediment diversions could be enhanced by the contribution of sand mining operations (so long as material is not dredged from the bed material source immediately upstream of the diversion) and dedicated bedload sediment traps. While the results of the present study are directly relevant to coastal restoration and river management issues in southeastern Louisiana, we believe the lessons learned and techniques used here can be applied in deltaic and coastal areas around the world facing increasing threat by rising sea level and climate change in the next century.

6. Conclusions

[52] 1. Estimates of skin-friction shear stress increased exponentially with water discharge, though substantial temporal and spatial variability in these estimates were observed at each measured discharge.

[53] 2. The morphology of the sand bars at Myrtle Grove and Magnolia evolved with flow conditions. The size and steepness of the bedforms covering both bars increased with water discharge from 18,000 to 27,000 $m^3 s^{-1}$ and decreased over the extended period of high-flow conditions from 27,000 to 32,000 $m^3 s^{-1}$. The extent of dune covered area at Myrtle Grove increased with water discharge, while remaining relatively unchanged at Magnolia.

[54] 3. For the water discharges measured during the present study (18,000–32,000 $m^3 s^{-1}$), the boundary between wash load sand and bed material sand is ~176 μm.(2).

[55] 4. Suspended sand loads measured using calibrated acoustic backscatter measurements compared favorably to sand loads measured using a more traditional isokinetic water sampler technique. These suspended sand load measurements directly correlated with water discharge following the relation of *Allison et al*. [2012], with the exception of a small

decrease in sand load at the highest measured water discharge ($32{,}000\,m^3\,s^{-1}$). Measured loads of suspended silt and clay did not correlate with water discharge, but rather followed a hysteresis cycle documented previously in the Mississippi River by *Mossa* [1996], *Galler and Allison* [2008], and *Allison et al*. [2012].

[56] 5. Concentrations of suspended sand increased with water discharge, and the location of maximum suspended sand concentration over the sand bars at Myrtle Grove and Magnolia coincided with the area of steepest bedforms, suggesting a complex feedback between flow conditions, channel-bed morphology, and bed material resuspension.

[57] 6. Rates of bed material sand transport associated with the migration of dunes increased exponentially with water discharge following the relations of *Nittrouer et al*. [2008], *Allison and Meselhe* [2010], and *Allison et al*. [2012], with the exception of anomalously low bedform transport rates measured at Myrtle Grove in May 2010 attributed to the removal of an upstream source of bed material by a dredging project. Repeated bathymetric measurements of the dredged area at Alliance revealed that bed material transport had replenished a substantial portion of the removed material.

[58] 7. River diversion projects seeking to utilize Mississippi River sediment must take into account the distinct transport pathways and source areas of wash load and bed material.

[59] **Acknowledgments.** This work was supported by the Louisiana Coastal Protection and Restoration Authority and the University of Texas Institute for Geophysics Maurice Ewing and J. Lamar Worzel Graduate Student Fellowship Program in Geophysics. We thank Marcy Davis, Dan Duncan, Alex Kolker, Ehab Meselhe, and Brian Vosburg for their assistance in the field and in preparing this manuscript. We also thank Alexander Densmore, John Pitlick, Ray Kostaschuk, and several anonymous reviewers for their thoughtful and detailed comments, which have greatly improved the quality of this manuscript.

References

Abdel-Fattah, S., A. Amin, and L. C. Van Rijn (2004), Sand transport in Nile River, Egypt, *J. Hydraul. Eng.*, *130*, 488–500, doi:10.1061/(ASCE)0733-9429(2004)130:6(488).

Allison, M. A., and E. A. Meselhe (2010), The use of large water and sediment diversion in the lower Mississippi River (Louisiana) for coastal restoration, *J. Hydrol.*, *387*, 346–360, doi:10.1016/j.jhydrol.2010.04.001.

Allison, M. A., C. R. Demas, B. A. Ebersole, B. A. Kleiss, C. D. Little, E. A. Meselhe, N. J. Powell, T. C. Pratt, and B. M. Vosburg (2012), A water and sediment budget of the lower Mississippi-Atchafalaya River in flood years 2008–2010: Implications for sediment discharge to the oceans and coastal restoration in Louisiana, *J. Hydrol.*, *432–433*, 84–97, doi:10.1016/j.jhydrol.2012.02.020.

Allison, M. A., B. M. Vosburg, M. T. Ramirez, and E. A. Meselhe (2013), Mississippi River channel response to the Bonnet Carré Spillway opening in the 2011 flood and its implications for the design and operation of river diversions, *J. Hydrol.*, *477*, 104–118, doi:10.1016/j.jhydrol.2012.11.011.

Bagnold, R. A. (1966), An approach to the sediment transport problem from general physics, *Geological Survey Professional Paper 422–1*, 42pp, United States Department of the Interior, Washington, D. C.

Barras, J., et al. (2003), Historical and Projected Coastal Louisiana Land Changes: 1978–2050, USGS Open File Report 03–334, 39 pp.

Bennett, S. J., and Best, J. L. (1995), Mean flow and turbulence structure over fixed, two-dimensional dunes: implications for sediment transport and bedform stability, *Sedimentol.*, *42*, 491–513, doi:10.1111/j.1365-3091.1995.tb00386.X.

Best, J. (2005), The fluid dynamics of river dunes: A review and some future research directions, *J. Geophys. Res.*, *110*, F04S02, doi:10.1029/2004JF000218.

Best, J., and R. Kostaschuk (2002), An experimental study of turbulent flow over a low-angle dune, *J. Geophys. Res.*, *107*(C9), 3135, doi:10.1029/2000JC000294.

Bianchi, T. S., and M. A. Allison (2009), Large-river delta-front estuaries as natural "recorders" of global environmental change, *Proc. Natl. Acad. Sci.*, *106*, 8085–8092, doi:10.1073/pnas.0812878106.

Biedenharn, D. S., C. R. Thorne, and C. C. Watson (2000), Recent morphological evolution of the lower Mississippi River, *Geomorphol.*, *34*, 227–249.

Carling, P. A., E. Golz, H. G. Orr, and A. Radecki-Pawlick (2000), The morphodynamics of fluvial sand dunes in the River Rhine near Mainz, Germany. I. Sedimentology and morphology, *Sedimentol.*, *47*, 227–252.

Church, M. (2006), Bed material transport and the morphology of alluvial river channels, *Annu. Rev. Earth Planet. Sci.*, *34*, 325–354, doi:10.1146/annurev.earth.33.092203.122721.

Church, J. A., and N. J. White (2006), A 20th century acceleration in global sea-level rise, *Geophys. Res. Lett.*, *33*, L01602 doi:10.1029/2005GL024826.

Crutzen, P. R. (2002), The "anthropocene", *J. Phys. IV*, *12*, 5, doi:10.1051/jp4:20020447.

Day, J. W., L. D. Britsch, S. R. Hawes, G. P. Shaffer, D. J. Reed, and D. Cahoon (2000), Pattern and process of land loss in the Mississippi Delta: a spatial and temporal analysis of wetland habitat change, *Estuaries*, *23*, 423–438.

Day, J. W., et al. (2007), Restoration of the Mississippi Delta: Lessons from Hurricanes Katrina and Rita, *Science*, *315*, 1679, doi:10.1126/science.1137030.

Demas, C. R., and P. B. Curwick (1987), Suspended-sediment, bottom-material, and associated-chemical data from the lower Mississippi River, Louisiana, Water Resources Basic Records Report 14, 117 pp.

Edwards, T. K., and G. D. Glysson (1999), Field methods for measurement of fluvial sediment, in *Techniques of Water-Resources Investigation of the U. S. Geological Survey, Book 3*, 97 pp., U.S. Geol. Surv., Reston, VA.

Einstein, H. A. (Sept. 1950), The bed-load function for sediment transportation in open channel flows, Tech. Bull., 1026, U.S. Dep. Of Agr., Washington, D.C.

Engelund, F., and J. Fredsøe (1982), Sediment ripples and dunes, *Annu. Rev. Fluid Mech.*, *14*, 13–37, doi:10.1146/annurev.fl.14.010182.000305.

Fredsøe, J. (1982), Shape and dimensions of stationary dunes in rivers, *J. Hydraul. Div., Am. Soc. Civ. Eng.*, *108*, 932–947.

Gagliano, S. M., K. J. Meyer-Arendt, and K. M. Wicker (1981), Land loss in the Mississippi River deltaic plain, *Trans. Gulf Coast Assoc. Geol. Soc.*, *31*, 295–300.

Galler, J. J., and M. A. Allison (2008), Estuarine controls on fine-grained sediment storage in the lower Mississippi and Atchafalaya Rivers, *Geol. Soc. Am. Bull.*, *120*, 386–398, doi:10.1130/B26060.1.

Garcia, M., and G. Parker (1991), Entrainment of bed sediment into suspension, *J. Hydraul. Eng.*, *117*, 414–435.

Gibbs, R. J., M. D. Matthews, and D. A. Link (1971), The relationship between sphere size and settling velocity, *J. Sediment. Petrol.*, *41*, 7–18, doi:10.1306/74D721D0-2B21-11D7-8648000102C1865D.

Gomez, B. (1991), Bedload transport, *Earth-Sci. Rev.*, *31*, 89–132.

Gomez, B., R. L. Naff, and D. W. Hubbel (1989), Temporal variation in bedload transport rates associated with the migration of bedforms, *Earth Surf. Processes Landforms*, *14*, 135–156.

IPCC (2007), *Climate Change 2007: The Physical Science Basis. Contribution of Working Group I to the Fourth Assessment Report of the Intergovernmental Panel on Climate Change*, edited by S. Solomon, D. Qin, M. Manning, Z. Chen, M. Marquis, K. B. Averyt, M. Tignor, and H. L. Miller, 996 pp., Cambridge University Press, Cambridge, UK and New York, NY.

Kim, W., D. Mohrig, R. Twilley, C. Paola, and G. Parker (2009), Is it feasible to build new land in the Mississippi River Delta? *Eos Trans. AGU*, *90*, 373–374.

Kostaschuk, R. (2000), A field study of turbulence and sediment dynamics over subaqueous dunes with flow separation, *Sedimentol.*, *47*, 519–531, doi:10.1046/j.1365-3091.2000.00303.X.

Kostaschuk, R., and P. Villard (1996), Flow and sediment transport over large subaqueous dunes: Fraser River, Canada, *Sedimentol.*, *43*, 849–863.

Kostaschuk, R., P. Villard, and J. Best (2004), Measuring velocity and shear stress over dunes with acoustic Doppler profiler, *J. Hydraul. Eng.*, *130*, 932–936, doi:10.1061/(ASCE)0733-9429(2004)130:9(932).

LACPRA (2012), *Louisiana's Comprehensive Master Plan for a Sustainable Coast, published by the Louisiana Coastal Protection and Restoration Authority (LACPRA)*, 170 pp., State of Louisiana, Baton Rouge, LA.

Lapointe, M. (1992), Burst-like sediment suspension events in a sand bed river, *Earth Surf. Processes Landforms*, *17*, 253–270, doi:10.1002/esp.3290170305.

Meade, R. H., and J. A. Moody (2010), Causes for the decline of suspended-sediment discharge in the Mississippi River system, 1940–2007, *Hydrol. Processes*, *24*, 34–49, doi:10.1002/hyp.7477.

Melis, T. S. (Ed.) (2011), *Effects of three high-flow experiments on the Colorado River ecosystem downstream from Glen Canyon Dam, Arizona*, 147 pp., USGS Circular 1366, U.S. Geol. Surv., Reston, VA.

Morton, R. A., J. C. Bernier, and J. A. Barras (2006), Evidence of regional subsidence and associated interior wetland loss induced by hydrocarbon production, Gulf Coast region, USA, *Environ. Geol.*, *50*, 261–274, doi:10.1007/s00254-006-0207-3.

Mossa, J. (1996), Sediment dynamics in the lowermost Mississippi River, *Eng. Geol.*, *45*, 457–479.

Nelson, J. M., and J. D. Smith (1989) Flow in meandering channels with natural topography, in *River Meandering*, edited by S. Ikeda, and G. Parker, pp. 69–102, AGU, Washington D. C.

Nicholls, R. J. (2004), Coastal flooding and wetland loss in the 21st century: changes under the SRES climate and socio-economic scenarios, *Glob. Environ. Change*, *14*, 69–86, doi:10.1016/j.gloenvcha.2003.10.007.

Nittrouer, J. A. (2006), Evaluation of bedload transport within the lower Mississippi River and its implications for sand discharge to the Gulf of Mexico, M.S. thesis, 68 pp., Tulane University, New Orleans, LA.

Nittrouer, J. A., M. A. Allison, and R. Campanella (2008), Bedform transport rates for the lowermost Mississippi River, *J. Geophys. Res.*, *113*, F03004, doi:10.1029/2007JF000795.

Nittrouer, J. A., D. Mohrig, and M. A. Allison (2011a), Punctuated sand transport in the lowermost Mississippi River, *J. Geophys. Res.*, *116*, F04025, doi:10.1029/2011JF002026.

Nittrouer, J. A., D. Mohrig, M. A. Allison, and A. B. Peyret (2011b), The lowermost Mississippi River: A mixed bedrock-alluvial channel, *Sedimentol.*, *58*, 1914–1934, doi:10.1111/j.1365-3091.2011.01245.X.

Nittrouer, J. A., J. L. Best, C. Brantley, R. W. Cash, M. Czapinga, P. Kumar, and G. Parker (2012), Mitigating land loss in coastal Louisiana by controlled diversion of Mississippi River sand, *Nat. Geosci.*, *5*, 534–537, doi:10.1038/NGEO1525.

Penland, S., and K. E. Ramsey (1990), Relative sea-level rise in Louisiana and the Gulf of Mexico: 1908–1988, *J. Coastal Res.*, *6*, 323–342.

van Rijn, L. C. (1984), Sediment transport, part II: Suspended load transport, *J. Hydraul. Eng.*, *110*, 1613–1641.

Roden, J. E. (1998), The sedimentology and dynamics of mega-dunes, Jamuna River, Bangladesh, Ph.D. dissertation, 340 pp., University of Leeds, Leeds, UK.

Schreider, M. I., and M. L. Amsler (1992), Bedforms steepness in alluvial streams, *J. Hydraul. Res.*, *30*, 725–743, doi:10.1080/00221689209498904.

Shugar, D. H., R. Kostaschuk, J. L. Best, D. R. Parsons, S. N. Lane, O. Orfeo, and R. J. Hardy (2010), On the relationship between flow and suspended sediment transport over the crest of a sand dune, Rio Parana, Argentina, *Sedimentol.*, *57*, 252–272, doi:10.1111/j.1365-3091.2009.01110.X.

Sime, L. C., R. I. Ferguson, and M. Church (2007), Estimating shear stress from moving boat acoustic Doppler velocity measurements in a large gravel bed river, *Water Resour. Res.*, *43*, W03418, doi:10.1029/2006WR005069.

Syvitski, J. P. M. (2005), Impact of humans on the flux of terrestrial sediment to the global coastal ocean, *Science*, *308*, 376, doi:10.1126/science.1109454

Syvitski, J. P. M., et al. (2009), Sinking deltas due to human activities, *Nat. Geosci.*, *2*, 681–686, doi:10.1038/ngeo629.

Topping, D. J., D. M. Rubin, and L. E. Vierra (2000), Colorado River sediment transport 1. Natural sediment supply limitation and the influence of Glen Canyon Dam, *Water Resour. Res.*, *36*, 515–542.

Topping, D. J., S. A. Wright, T. S. Melis, and D. M. Rubin (2007), High-resolution measurements of suspended-sediment concentration and grain size in the Colorado River in Grand Canyon using a multi-frequency acoustic system, *Proc. 10th Int. Symp. River Sediment.*, *3*, 330–339.

Törnqvist, T. E., D. J. Wallace, J. E. A. Storms, J. Wallinga, R. L. van Dam, M. Blaauw, M. S. Derksen, C. J. W. Klerks, C. Meijneken, and E. M. A. Snijders (2008), Mississippi Delta subsidence primarily caused by compaction of Holocene strata, *Nat. Geosci.*, *1*, 173–176, doi:10.1038/ngeo129.

Venditti, J. G., and S. J. Bennett (2000), Spectral analysis of turbulent flow and suspended sediment transport over fixed dunes, *J. Geophys. Res.*, *105*, 22035–22047, doi:10.1029/2000JC900094.

Yalin, M. S., and E. Karahan (1979), Steepness of sedimentary dunes, *J. Hydraul. Div. Am. Soc. Civ. Eng.*, *104*, 381–392.